NASA TECHNICAL NOTE

NASA TN D-6910

NASA TN D-6910

FLIGHT TEST OF AN ERECTABLE SPACECRAFT USED FOR DECELERATOR TESTING AT SIMULATED MARS ENTRY CONDITIONS

by Allen B. Henning and Reginald R. Lundstrom

Langley Research Center
Hampton, Va. 23365

NATIONAL AERONAUTICS AND SPACE ADMINISTRATION • WASHINGTON, D. C. • OCTOBER 1972

1. Report No.	2. Government Accession No.	3. Recipient's Catalog No.
NASA TN D-6910		

4. Title and Subtitle	5. Report Date
FLIGHT TEST OF AN ERECTABLE SPACECRAFT USED FOR DECELERATOR TESTING AT SIMULATED MARS ENTRY CONDITIONS	October 1972
	6. Performing Organization Code
7. Author(s)	8. Performing Organization Report No.
Allen B. Henning and Reginald R. Lundstrom	L-8595
	10. Work Unit No.
9. Performing Organization Name and Address	117-07-04-01
NASA Langley Research Center Hampton, Va. 23365	11. Contract or Grant No.
	13. Type of Report and Period Covered
12. Sponsoring Agency Name and Address	Technical Note
National Aeronautics and Space Administration Washington, D.C. 20546	14. Sponsoring Agency Code

15. Supplementary Notes

With appendix A by James C. Young

16. Abstract

A 16.76-meter-diameter (55-ft) disk-gap-band parachute was deployed behind an expandable 4.57-meter-diameter (15-ft), 120° blunted-cone simulated spacecraft. The spacecraft was carried to altitude in the folded condition. An automatic control system kept the folded spacecraft pointing in the desired direction after booster separation. The aeroshell was then erected at the desired conditions by ground command. When the desired parachute test conditions were reached, another ground command deployed the test parachute. The test Mach number and dynamic pressure obtained at the parachute peak load were 2.62 and 929 N/m^2 (19.4 lbf/ft^2), respectively. A large disturbance after aeroshell erection caused a large angle of attack to exist at parachute deployment. Methods of preventing this disturbance are discussed.

17. Key Words (Suggested by Author(s))	18. Distribution Statement
Parachute test vehicle Mars entry Blunt body Erectable spacecraft	Unclassified – Unlimited

19. Security Classif. (of this report)	20. Security Classif. (of this page)	21. No. of Pages	22. Price*
Unclassified	Unclassified	57	$3.00

*For sale by the National Technical Information Service, Springfield, Virginia 22151

FLIGHT TEST OF AN ERECTABLE SPACECRAFT USED FOR DECELERATOR TESTING AT SIMULATED MARS ENTRY CONDITIONS

By Allen B. Henning and Reginald R. Lundstrom
Langley Research Center

SUMMARY

A flight test has been conducted on an erectable 4.57-meter-diameter (15-ft), 120° blunted-cone vehicle capable of testing large decelerators under simulated Mars entry conditions at a desired Mach number and dynamic pressure. A disk-gap-band parachute with a 16.76-meter (55-ft) nominal diameter was deployed as the experimental decelerator behind the test vehicle. The desired test requirements for this experimental parachute were a Mach number of 2.70 and a dynamic pressure of 1005 N/m^2 (21 lbf/ft^2). The test point obtained at the parachute peak load was a Mach number of 2.62 and a dynamic pressure of 929 N/m^2 (19.4 lbf/ft^2). After aeroshell erection and nose-cone separation, a disturbance produced a large oscillation in the attitude of the aeroshell-payload combination. Postflight studies showed that the disturbance was caused by the wake of the separated nose cone impinging on the aeroshell. The dynamic stability and drag parameters of the aeroshell-payload combination observed in flight agreed well with referenced data.

INTRODUCTION

Aerodynamic decelerators which could be suitable to absorb a large amount of kinetic energy during entry into a Mars atmosphere have been the subject of many investigations. (For example, see refs. 1 and 2.) Concern has been expressed as to how the inflation characteristics and stability of such decelerators are affected by their being deployed behind a large blunt body that might represent a typical Mars entry configuration. A description of a flight test system used for full-scale parachute tests behind a blunt body at Mach numbers up to 1.6 is presented in references 3 and 4. The results of wind-tunnel tests in which a survey was made of the dynamic pressures in the wake behind some typical spacecraft configurations are presented in reference 5.

Although the above-mentioned parachute tests indicate little difference in opening characteristics whether or not the decelerator tests are made behind a blunt body, considerable concern exists about the stability of the system after parachute opening, partic-

ularly at Mach numbers above 1.6. During the tests behind a blunt body reported in reference 2, the large-diameter body was released immediately after parachute inflation and the aeroshell and payload-parachute combination separated very rapidly; hence, the stability data on the complete system were not obtained. Also, as more data became available on the performance requirements for Mars entry, parachute test results at Mach numbers higher than 1.2 and 1.6, which were the test Mach numbers of references 3 and 4, became of interest.

In order to perform tests in the Mach number range of 1.2 to 4.0 by use of the system described in references 3 and 4, considerable redesign is required. There would be considerable advantage in designing a test system that could perform at any desired condition within this range by making simple adjustments, such as amount of ballast carried, angle of launch, or times during the trajectory at which specified events are made to occur. The versatility of such a test system would make it a valuable tool in conducting general research throughout this test range.

The system used for the experiment covered by this report consists of a rocket-powered vehicle and an erectable device which in the expanded condition simulates a planetary spacecraft. The simulated spacecraft is propelled to altitude in a folded condition. During reentry it is opened to a 120° blunted cone to form the simulated spacecraft. When the desired Mach number and dynamic pressure are reached, the decelerator test is performed. Variation in performance is attained by adjusting the amount of ballast carried in the thrusting stage and/or on the spacecraft and by varying the altitude at which the spacecraft is erected. This vehicle was capable of making a decelerator test behind a blunt body over a Mach number range of 1.2 to 4.0 and at dynamic pressures up to 1440 N/m^2 (30 lbf/ft^2).

A flight test was conducted at NASA Wallops Station to determine the opening and stability characteristics of a disk-gap-band parachute when opened in the wake of a blunt body and to determine the performance of the erectable simulated spacecraft used as the parachute test vehicle. A complete description of the parachute and its performance as determined from the test is not included in this report but is presented in reference 6. The purpose of this report is to describe the erectable spacecraft and to present its flight test results. This report also contains an appendix describing the automatic control system used on the vehicle and an appendix analyzing an anomaly in performance encountered during the flight.

SYMBOLS

Measurements are given in the International System of Units (SI) with the equivalent values in U.S. Customary Units indicated in parentheses. The principal measurements and calculations were made in U.S. Customary Units.

C_l rolling-moment coefficient, $\frac{\text{Rolling moment}}{qSd}$

C_{l_p} damping-in-roll derivative, $\frac{\partial C_l}{\partial(pd/2V)}$, per radian

C_{l_δ} roll derivative, $\frac{\partial C_l}{\partial \delta}$, per radian

C_m pitching-moment coefficient about center of gravity, $\frac{\text{Pitching moment}}{qSd}$

C_{m_α} slope of pitching-moment-coefficient curve, $\frac{\partial C_m}{\partial \alpha}$, per radian

C_{m_q} damping-in-pitch derivative, $\frac{\partial C_m}{\partial(q'd/2V)}$, per radian

C_N normal-force coefficient, $\frac{\text{Normal force}}{qS}$

C_{N_α} slope of normal-force-coefficient curve, $\frac{\partial C_N}{\partial \alpha}$, per radian

C_X axial-force coefficient, $\frac{\text{Axial force}}{qS}$

d reference diameter, meters (feet)

g acceleration due to gravity, 9.805 m/sec^2 (32.17 ft/sec^2)

h altitude, meters (feet)

M Mach number

m mass, kilograms (slugs)

p rolling velocity, radians/second

q dynamic pressure, newtons/meter^2 (pounds-force/foot^2)

q' pitching velocity, radians/second

S reference area, meters^2 (feet^2)

t	time, seconds
V	velocity, meters/second (feet/second)
x_{cg}	vehicle center of gravity, origin as noted in table IV, meters (feet)
x_{cp}	vehicle center of pressure, origin as noted in table IV, meters (feet)
α	angle of attack, degrees
β	angle of sideslip, degrees
δ	fin deflection, radians
η	total angle of attack, degrees

DESCRIPTION OF TEST

The objectives of the flight test were (1) to determine the opening and stability characteristics of a 16.76-meter-diameter (55-ft) disk-gap-band parachute when opened in the wake of a simulated spacecraft configuration and (2) to evaluate the performance of an erectable 4.57-meter-diameter (15-ft), 120^{o} blunted-cone spacecraft configuration as a vehicle for testing parachutes. Weight and event times for this test were adjusted so that the erected aeroshell-payload combination with a ballistic coefficient m/C_XS of 47.13 kg/m^2 (0.30 $slug/ft^2$) would enter a simulated minimum Mars atmosphere (ref. 7) and at parachute peak load would attain a Mach number of 2.70 and a dynamic pressure of 1005 N/m^2 (21 lbf/ft^2).

Sequence of Events

An illustration of the planned sequence of events from launch to splashdown for a nominal trajectory is presented in figure 1. The expected times, altitudes, dynamic pressures, and Mach numbers are shown in the illustration.

Since a variety of off-nominal trajectories are possible, the spacecraft trajectory is carefully monitored, both visually on the radar plotting board and by a digital computer, and is compared with predetermined trajectories. At a preselected altitude after burnout, the computer calculates the time of aeroshell erection using the velocity and flight-path angle obtained from real-time radar data. This calculation optimizes the erection time for any trajectory in order to obtain the test conditions of Mach number and dynamic pressure at parachute peak load. This time varies for each possible trajectory, but for the

nominal trajectory, the erection time is 220 seconds at a dynamic pressure of 24 N/m^2 (0.5 lbf/ft^2). The mortar fires to deploy the parachute so that it is fully opened at a nominal dynamic pressure of 1005 N/m^2 (21 lbf/ft^2) and a Mach number of 2.70. The aeroshell and the payload ballast weight separate from the payload. The payload is buoyant and floats in the water after splashdown. Both payload and parachute are recovered by skindivers and a helicopter.

Command System

From the test conditions it is desired that the parachute reach its fully opened condition at the moment that the dynamic pressure is 1005 N/m^2 (21 lbf/ft^2). Because of the normal trajectory dispersion to be expected, this dynamic-pressure value will not occur at the same time for each possible trajectory. Therefore, instead of time being the criterion for parachute deployment, a computer-initiated command system is set up to fire a mortar to deploy the parachute at the proper dynamic pressure. Also, as stated previously, the aeroshell erection time for optimum Mach number and dynamic-pressure test conditions can vary; hence, the command system is also utilized for initiating the aeroshell erection.

In order to determine the dynamic pressure experienced by the spacecraft, a computer working in conjunction with the radar is utilized to calculate, smooth, and extrapolate the incoming trajectory data. The radar supplies the computer with the spacecraft position data every 0.1 second, and the computer calculates the dynamic pressure experienced by the spacecraft at that time. These data are used in a least-squares method to fit a second-order curve through the last n number of points. It was found by trial and error that 75 is the minimum number of points that could be used to fit the second-order curve that would be free of large errors which could be generated from noisy data. The 75 points advanced along with each new data point. With the polynomial the computer predicts ahead 1.64 seconds, and when the proper dynamic pressure is predicted, a signal is sent via the command system to the spacecraft. The predict-ahead time of 1.64 seconds is composed of several quantities, such as time for computer calculations, relay closures, camera starting delay, mortar firing, parachute line stretch, and parachute opening. Several trajectory simulations were run before the test flight to obtain the best estimate of this time. A command signal to erect the aeroshell is also sent by the computer. This command is sent on the basis of the calculated erection time or, in case of a very low trajectory, on an aerodynamic limit not to exceed a dynamic pressure of 192 N/m^2 (4.0 lbf/ft^2), whichever comes first. A third command is sent manually to release the payload ballast after descent to about 4572 meters (15 000 ft).

A knowledge of the atmospheric temperature and pressure at the time of launch is necessary in order to calculate and predict the dynamic pressure that the spacecraft is or

will be experiencing. Twenty-four hours before the test flight an Arcasonde was launched to obtain high-altitude density data that were incorporated into the computer and used in the calculation of dynamic pressure. According to reference 8, the density data taken 24 hours before the test reduced the uncertainty over density measured earlier in the day for an afternoon test.

VEHICLE DESCRIPTION

The description of the total test vehicle is presented in two parts: (1) the propulsion system, which includes the boost system, the interstage, and the despin system, and (2) the folded spacecraft, which consists of the nose cone, the erectable aeroshell, and the payload. Sketches of the total vehicle and its component parts are presented in figures 2 and 3. A photograph of the total vehicle on the launcher is presented in figure 4.

Propulsion System

The test vehicle was powered by a Castor XM-33E2 rocket motor with two Recruit TE-M-29-1 assist rocket motors attached to the side of the Castor. The Recruits burned for 2.4 seconds and assisted the Castor during the initial phase of the flight to increase the take-off acceleration and thereby decrease the trajectory dispersion due to winds. Each fin of the four-fin assembly had a nominal exposed area of 1.116 m^2 (12 ft^2) and was made of cast magnesium with a leading-edge cap of inconel for protection from aerodynamic heating. Each fin was mounted to a cast magnesium shroud, and the incidence was made adjustable to zero with a tolerance of less than $\pm 0.05^{\circ}$.

The despin system, which was activated 60 seconds after take-off, was designed to eliminate any roll the vehicle might have acquired because of asymmetries in construction and thrust misalinements. It positioned the vehicle to the desired roll orientation for initiation of the spacecraft attitude control system immediately after booster separation. The attitude gyros in the spacecraft served the dual purpose as a reference for the despin system as well as for the automatic control system. The installation of the jets and associated hardware for the despin system may be seen in figure 5, and a more complete description of the system may be found in appendix A.

The spacecraft and booster were locked together with a V-clamp coupling using explosive bolts, and when this clamp was released, the parts were restrained by a captive system and stayed with the booster section throughout the rest of the flight. A separation bellows located in the forward end of the interstage imparted a separation velocity of about 3 m/sec (10 ft/sec) between the spacecraft and booster after release of the clamp.

Also included in the interstage was a ballast weight of 377 kg (831 lbm), which was added to the test vehicle so that the desired test Mach number and dynamic pressure would be obtained.

Spacecraft

The simulated spacecraft consisted of a nose cone and an entry configuration which included an erectable aeroshell and a payload, herein referred to as the aeroshell-payload section. The payload contained the instrumentation section, the parachute mortar, the parachute, and ballast. Details of the configurations may be seen in figure 3.

Nose cone.- The nose cone was a 10^{o} half-angle fiber glass cone with a 5.08-cm-radius (2-in.) steel tip. It served as a heat shield and housed the erection system and its nitrogen supply tanks, the nitrogen supply for the spacecraft attitude control system, the control valves, and the pitch, yaw, and roll jets. The supply tank for the erection system held 0.029 m^3 (1.024 ft^3) of nitrogen at 7860 kN/m^2 (1140 lbf/in^2).

The nose cone was attached to the front part of the aeroshell with three pyrotechnic release nuts which were fired when the aeroshell was locked in the opened position. A description of the aeroshell erection system, its design and analysis is presented in reference 9. When the aeroshell was erected and the nose cone had been released from the aeroshell, the residual gas in the erection system pushed the nose cone away from the aeroshell with an initial separation velocity of about 3 m/sec (10 ft/sec). It continued on ahead of the rest of the spacecraft because of its higher ballistic coefficient. The complete erection system and the control-system jets were jettisoned with the nose cone. A row of stainless steel, flexible shingles covered the junction of the nose cone and the sides of the folded aeroshell. The flexibility of the shingles prevented them from restraining the sides of the aeroshell during erection. In figure 6 the shingles are shown on the folded and erected aeroshell. They were attached to the nose cone and separated with it.

Aeroshell.- The aeroshell was an erectable structure with a framework of 24 aluminum alloy ribs attached to a central hub. A photograph showing the ribs mounted in the hub is shown in figure 7. A detailed description and analysis of the erecting arms and the ribs is presented in reference 9. The framework of ribs was covered with 285-g/m^2 (8.4-oz/yd^2) Nomex fabric. This fabric was prestretched when installed and made the erected aeroshell essentially a rigid unit. The Nomex was covered with a coating of Viton PLV 2002 to reduce its porosity. Cap strips of fiber glass were fastened to the top of each rib over the Nomex. These strips had tongue-and-groove edges so that the Nomex was not exposed to the airstream when the aeroshell was in the folded condition. The cap strips were flat with the edges somewhat beveled so that the cross section of the folded aeroshell was a 48-sided polygon with a diagonal of 78.7 cm (31 in.) rather than a circle. The ribs were held in the folded position by a 3.18-mm (0.125-in.) cable placed in grooves at the end of each rib. A photograph showing the rib ends, the fiber glass cap strips, and the cable is presented in figure 8. Two cable cutters cut the cable just before aeroshell erection. When fully erected, the aeroshell formed a sharp-edged 120^{o} blunted cone, 4.57 meters (15 ft) in diameter with a smooth nose radius of 73.0 cm (28.75 in.). In the

opened position the fiber glass strips protruded about 0.64 cm (0.25 in.) above the tightly stretched Nomex fabric.

Payload.- The payload was joined to the aeroshell by a V-clamp coupling and consisted of the instrumentation section, the parachute mortar, the parachute, and ballast. The structure was fabricated of aluminum alloy and had a watertight compartment that housed the instrumentation section. The clamp holding the payload and aeroshell together was released by explosive bolts. The pieces of the clamp were retained with the aeroshell. A sketch of the payload is shown in figure 3.

The instrumentation of this vehicle consisted of the telemetry system, radar transponder and beacon system, the command system, the guidance system, and the camera system. An 18-channel FM/FM VHF telemetry system continuously transmitted the data from the vehicle to the ground receiving station through four of the eight spike antennas at the rear of the payload. The antenna locations and arrangement are shown in the photograph of figure 9. The continuously telemetered data consisted of three tensiometer measurements; four accelerations; yaw, pitch, and roll attitude; on-off signal to the yaw, pitch, and roll jets from the control system; erection-chamber pressure; two command-receiver on-off monitors; camera correlation timer; and one channel of commutated data. The commutated data consisted of supply and jet pressures and functions of the attitude control system, erection-system pressures, course pitch and yaw attitude, vehicle and spacecraft separations, internal battery monitors, and command-receiver on-off monitors. The vehicle incorporated a C-band radar tracking transponder to aid radar tracking of the spacecraft throughout the flight. Recovery beacons were used for locating the vehicle after impact in the water. Two command-receiver systems, each independent of the other, were used for commands from the ground station to erect the aeroshell, deploy the parachute, and release the payload ballast. The guidance or attitude control system consisted of gyros that sensed a change in yaw, pitch, and roll and sent a signal to the control system that corrected the attitude change by expelling compressed nitrogen gas through the proper jets. A description of the attitude control system is presented in appendix A. Vehicle attitude was telemetered from the attitude gyros throughout the flight. The camera system consisted of four Milliken DBM-25 High "G" cameras. Two cameras looking rearward photographed the performance of the parachute, one camera looking out the side of the payload monitored the aeroshell erection and the horizon, and one camera looking forward monitored the aeroshell-payload separation. Camera locations are shown in figure 3. All cameras not in the watertight instrument compartment were in individual watertight containers.

The parachute mortar was in the rear section of the payload and had a capacity of 0.088 m^3 (3.12 ft^3). It was designed to deploy a weight of 57.6 kg (127 lbm) at a muzzle velocity of 46.9 m/sec (154 ft/sec). The packed parachute bag was placed in the mortar

tube on a push plate (sabot) with the closed end of the bag attached to the cover of the mortar tube.

The parachute used in this flight test was a disk-gap-band parachute. A sketch of the parachute-payload system is presented in figure 10. A complete description of this parachute is given in reference 6. The basic parachute characteristics are as follows:

Nominal diameter, m (ft)	16.76 (55)
Nominal area, m^2 (ft^2)	220.7 (2376)
Number of gores and suspension lines	42
Total geometric porosity, percent of area	12.5
Suspension-line length, m (ft)	16.76 (55)
Riser length, m (ft)	2.93 (9.6)

The ballast weight, which is illustrated in the sketch of the payload in figure 3, was released by explosive bolts on command before the payload and parachute hit the water.

PREFLIGHT TESTING

In preparing the spacecraft for flight, all the various components and systems in the spacecraft went through qualification tests to assure reliability. The aeroshell erection system, the parachute mortar, the attitude control system, the separation devices, and the antennas were subjected to extensive qualification testing. Vibration and shock tests were performed to simulate various in-flight events such as rocket-motor ignition, rocket-motor burning, booster-spacecraft separation, and nose-cone separation. A high-speed aeroshell-erection shock test and a mortar-firing shock test both were carried out in a vacuum chamber to closely simulate flight atmospheric conditions. Recovery operations were practiced in order to determine the most efficient way of recovering the payload and parachute from the water.

ACCURACY

The estimated accuracy of the data from the spacecraft instrumentation and the measured quantities from ground-based radar are presented in table I. The best error estimate represents the known accuracy of some components, experience from the use of other components, and scatter in the data. The estimated errors presented in table I are especially applicable to flight conditions in an altitude range of about 39.6 km (130 000 ft) to 57.9 km (190 000 ft).

The instrumentation errors were compiled from several factors characteristic of the instrument. The error in yaw, pitch, and roll is based mainly on gyro drift from the time the gyro is uncaged to the time of aeroshell erection.

The space position data were obtained from the FPS-16 and FPQ-6 radar units, and comparison of the data from these two independent data sources showed that the difference was very small. Similarly, the velocity obtained by differentiating the space position with time on all radars was plotted and compared. The velocity values used in the data were calculated by vectorially adding the velocity values obtained from radar to the velocity of the high-altitude winds measured with an Arcas sounding rocket.

The local atmospheric conditions were obtained from a rawinsonde from 0 to 29 km (94 500 ft) and by an Arcasonde from 29 to 51 km (94 500 to 167 000 ft). Data needed above that altitude were extrapolated by using the U.S. Standard Atmosphere, 1962 (ref. 10) as a guide.

FLIGHT TEST RESULTS AND DISCUSSION

Data from the flight test will be presented and discussed in the following four sections: (1) launch to booster separation, 0 to 90.08 seconds, (2) booster separation to aeroshell erection, 90.08 to 224.5 seconds, (3) aeroshell erection to mortar fire, 224.5 to 240.3 seconds, and (4) mortar fire through aeroshell-payload separation to impact, 240.3 to 1655 seconds.

A plot of the density data measured 24 hours before the test flight that were used for the dynamic-pressure predictions is shown in figure 11 along with data from the U.S. Standard Atmosphere, 1962 (ref. 10) and the postflight data. The postflight density data were measured by Arcasonde about 2 hours after the flight and at the test altitude were about 5 percent less than the data measured 24 hours before the test flight.

The mass characteristics of weight, center of gravity, and moments of inertia for the total vehicle and various vehicle configurations that occur during the flight are presented in table II. The estimated variation in mass characteristics of the total vehicle during the thrusting period are presented in table III. The estimated aerodynamic characteristics used for preflight calculations and postflight simulations are presented in table IV. The total vehicle normal-force coefficient was derived from references 11, 12, and 13; pitching moment and pitch damping from reference 14; rolling moment and roll damping from references 15 and 16. The normal-force coefficient and center of pressure of the folded spacecraft were derived from reference 17. The aerodynamic coefficients of normal force, axial force, and center of pressure for the erected aeroshell were obtained from reference 18. The pitch damping of the erected aeroshell obtained from reference 19 was assumed to be constant over the angle-of-attack and Mach number range quoted herein. The estimated drag curves for the total flight configuration and folded spacecraft are presented in figure 12. These drag curves were derived in part from data in references 13 and 20. All these estimated aerodynamic characteristics were used in the preflight analysis of this vehicle.

The overall trajectory of the aeroshell, payload, and booster is presented in figure 13 along with the predicted trajectory of the payload from launch to impact. Table V compares the nominal and the actual time, Mach number, dynamic pressure, and altitude for significant flight events. It can be noted in figure 13 that the actual flight trajectory is lower in altitude at apogee than the predicted trajectory. Since the drag, thrust, and launch angle are some of the variables that will change the trajectory, a variation of these parameters was made to reconstruct the actual flight trajectory. The results of this investigation indicate that the thrust of the vehicle was below nominal for the Castor rocket motor. This lower thrust results in a lower apogee and a lower Mach number for the parachute test conditions. At 90.08 seconds the Castor rocket motor was separated from the spacecraft and was skin tracked by the SPANDAR radar. In figure 13 the tracks of both are shown to be in proximity to one another throughout the trajectory. After the aeroshell had erected and its drag had increased, the booster passed the aeroshell-payload so that there was a separation of about 579 meters (1900 ft) between the two configurations at mortar firing, and the distance increased at the rate of about 213 m/sec (700 ft/sec). Thereby, the booster was prevented from interfering with the parachute test. The booster impacted at approximately 300 seconds. During the test sequence the aeroshell was separated from the payload-parachute combination and was skin tracked by radar. As the payload-parachute descended through the atmosphere it was influenced by the winds; therefore, the track of the payload-parachute was quite erratic. About 4907 meters (16 100 ft) altitude the ballast was released, and therefore, the rate of descent of the payload-parachute decreased.

Launch to Booster Separation, 0 to 90.08 Seconds

The wind speed and direction were measured for wind weighting purposes from 0 to 27 km (90 000 ft) to cover the entire thrusting altitude range of the Castor rocket motor. The wind compensation method of reference 21 was used to obtain the launcher settings. The zero reference for the automatic control system (appendix A) required that the vehicle be positioned on the launcher at 90° elevation angle for gyro uncaging. The underside of the vehicle was directed toward the wind-corrected launch azimuth (178.0°). The gyros were uncaged at about -2 minutes. The launcher was then lowered to the wind-corrected launch elevation angle (81.1°) and launched. At the end of the Castor burnout, the vehicle was on the nominal 80° trajectory and an azimuth heading of 158.3° compared with a nominal azimuth of 158°. The vehicle had a little lower than nominal velocity.

The time history of the longitudinal acceleration during the rocket-motor burning is presented in figure 14. The variation of velocity, Mach number, flight-path angle, and altitude with time during this period is shown in figures 15 and 16. The dynamic pressure is presented in figure 17.

Because of fin construction asymmetries and thrust misalinements, a slight roll was generated during the thrusting period. The roll-rate time history is presented in figure 18. At 60.15 seconds the despin system was activated to despin and orient the vehicle to the proper roll attitude for initiation of the spacecraft control system after separation. The vehicle roll rate decreased to a constant 12.5 deg/sec until it neared the proper roll attitude; then the roll gradually decreased until the zero roll position had been obtained. About 10 seconds was required to despin and orient the vehicle to zero roll position. This position was held through aeroshell erection.

The behavior of the vehicle attitude after burnout through booster separation is shown by the variation of pitch attitude angle, flight-path angle, and yaw attitude angle with time in figure 19. At 79 seconds the pitch and yaw attitude reference by the automatic control system was accomplished by reading the gyro attitude angles and storing for future reference. The reading for pitch was 52° and for yaw was -6.3°.

At 90.08 seconds the booster separated from the spacecraft without any apparent disturbance. The separation bellows was fully extended at 90.16 seconds and separation was completed. The radar track of the booster is shown in figure 13.

Booster Separation to Aeroshell Erection, 90.08 to 224.5 Seconds

After the booster separated from the spacecraft, the pitch and yaw jets in the spacecraft were turned on at 90.45 seconds, and the control system oriented the spacecraft toward the attitude position measured at 79 seconds. The dynamic pressure was less than 38 N/m^2 (0.8 lbf/ft^2), so very little aerodynamic force was acting on the vehicle. The control system positioned the spacecraft to a pitch attitude of 54° and a yaw attitude of -5.2°, which were within the $\pm 2^{\circ}$ dead band of the referenced attitudes at 79 seconds. (See fig. 19.) The dead bands are regions where the pitch and yaw jets are inactive. (See appendix A.) The vehicle was held inside the pitch and yaw dead bands until 145 seconds when an attitude change maneuver started. At this time the sign of the pitch and yaw attitude reference was changed (appendix A), and the automatic control system started to turn the vehicle so that it would be oriented to its new pitch attitude angle of -52° and new yaw attitude angle of $+6.3^{\circ}$.

The attitude maneuver and the control dead bands are shown in figure 20. The telemetry record of both the pitch and yaw attitude angles and the on-off pitch and yaw control jet traces indicates that the pitch and yaw attitudes followed the edges of their respective dead bands throughout most of the control period. After the attitude reference change, the dead bands of both the pitch and yaw controls had been displaced and narrowed, as shown in figure 20. The small apparent displacement of the dead bands could be attributed to the accumulation of possible errors in the automatic control system, which include potentiometer misalinements, calibration zero shifts, and voltage changes. The narrow-

ing of the dead bands could be caused by noise in the dead-band control circuitry. A few seconds before aeroshell erection (from about 218 seconds) the pitch and yaw attitude angles gradually increased beyond the apparent dead-band limits. This increase indicates that the spacecraft aerodynamic moments were about equal to or greater than the control-system jet moments. Just before aeroshell erection at 224.5 seconds the readout from the yaw attitude gyro indicated an angle of 11.1°, and the readout from the pitch attitude gyro indicated an angle of -53.1°. Trajectory data, including dynamic pressure, velocity, Mach number, altitude, and flight-path angle, for the time period before aeroshell erection through the parachute test are presented in figures 21 and 22.

A rough estimate of the vehicle attitude conditions with respect to the direction of flight at aeroshell erection can be determined from the pitch and yaw attitude gyro. Because of the azimuth shift (due to winds) directly after launch, the yaw attitude gyro indicated an average angle of -6.8° just before separation. Since the vehicle heading was in the direction of flight, the indicated -6.8° was actually a zero yaw angle. (The yaw reference value at 79 seconds of -6.3° (fig. 19) differed from -6.8° because of a slight attitude oscillation about the flight path.) After the attitude change maneuver and just before aeroshell erection, the yaw attitude gyro indicated an angle of 11.1° while the direction of flight remained essentially unchanged. Therefore, an estimated angle in the yaw plane between the spacecraft axis and the relative wind at 224.5 seconds was 17.9°. This large yaw attitude angle could have been greatly reduced if the automatic control system had been designed so that the yaw attitude would not change during the attitude maneuver. At 224.5 seconds the pitch attitude gyro indicated an attitude of -53.1°, and when compared with the flight-path angle of -56.5° from figure 22, an estimated angle of 3.4° results in the pitch plane.

Aeroshell Erection to Mortar Fire, 224.5 to 240.3 Seconds

As mentioned previously, the computer was programed to send the aeroshell erection command at an in-flight calculated time for the type of trajectory followed or at a limit dynamic pressure of 192 N/m^2 (4.0 lbf/ft^2), whichever occurred first. Since the trajectory flown was a low trajectory, the command was sent when the computer estimated the dynamic pressure to be 192 N/m^2 (4.0 lbf/ft^2). Postflight analysis of the dynamic pressure (fig. 21) shows that the aeroshell erected at a dynamic pressure of 180 N/m^2 (3.76 lbf/ft^2) at 224.5 seconds.

When the aeroshell was completely erected, the explosive nuts holding the nose cone to the aeroshell fired and released the nose cone. The jets of the automatic control system were separated with the nose cone; therefore, no jet forces could be applied to the aeroshell-payload configuration after nose-cone separation. As the nose cone fell away from the aeroshell, a disturbance caused the aeroshell to oscillate to a very large amplitude in a direction opposite to the total attitude angle the spacecraft experienced before

erection. The raw gyro attitude data with respect to the inertial axis system show this oscillation in figure 23. Possible causes of this disturbance were the large attitude angle at aeroshell erection and the influence of the wake of the separated nose cone creating a low-pressure area immediately behind the nose cone on part of the aeroshell surface; thus unbalanced pressure areas would be produced. A study, presented in appendix B, using postflight wind-tunnel data of the wake of the separated nose cone impinging on the aeroshell (ref. 22) showed that the nose cone did affect the aeroshell. This study indicated that the disturbance experienced by the aeroshell could have been minimized by erecting the aeroshell and releasing the nose cone near zero dynamic pressure.

By the method of reference 23, the raw gyro attitude data of figure 23 were transformed into angles of attack and sideslip with respect to a rolling body axis system through several axis rotations considering the attitude at which the gyro was uncaged, the launcher settings, and the vehicle flight path. The resulting α and β are presented in figure 24. Just before aeroshell erection at 224.5 seconds, the angle of attack and angle of sideslip were 6° and 20°, respectively. This produced a total angle with respect to the flight path of about 21° at time of aeroshell erection and contributed to the oscillation caused by the nose-cone wake.

In the transformation method to reduce the gyro attitude data to α and β for figure 24, no correction was made for possible gyro drift. Therefore, the oscillations of α and β do not center about zero, but about some other value. The oscillation center line provided a reference for further analysis. The time period selected for further analysis was 231.0 and 240.0 seconds to avoid any possible nose-cone interference in the data. A total angle of attack η was calculated by using the relationship

$$\cos \eta = \cos \alpha \cos \beta$$

A plot of η is presented in figure 25. This curve shows some damping, and the time to damp to 1/2 the amplitude is estimated to be 15.5 seconds. The Mach number during this time varies from 2.68 to 2.72, and the magnitude of the oscillation ranges from a high of 61.8° at 231.1 seconds to a low of 42° at 239.3 seconds. From six-degree-of-freedom simulations the average C_{m_q} over this large total-angle-of-attack range was determined to be -0.51 with an average x_{cp}/d of 1.127 and an x_{cg}/d of 0.222. These measurements are referred to the 120° cone apex. The Reynolds number is on the order of 500 000. The value of C_{m_q} obtained here compares well with C_{m_q} values from reference 24 for a 120° cone with similar physical parameters. The drag coefficient obtained from the data of the longitudinal accelerometer when the aeroshell-payload was at or near zero angle of attack was 1.52 at $M = 2.70$. This value is comparable with the value of drag that was used for preflight calculations.

At 240.3 seconds when the mortar fired, the aeroshell-payload oscillation had damped so that the total angle of attack was about 40^{o}.

Mortar Fire to Splashdown, 240.3 to 1655 Seconds

At 239.74 seconds the computer predicted that a dynamic pressure of 1005 N/m^2 (21 lbf/ft^2) would be reached at the time of parachute peak load and sent the second command signal. This signal was received at 239.80 seconds, and at 240.31 seconds the mortar fired to deploy the parachute. The mortar fired at a dynamic pressure of 873 N/m^2 (18.24 lbf/ft^2) and a Mach number of 2.69. The results obtained at peak load were a dynamic pressure of 929 N/m^2 (19.4 lbf/ft^2) at a Mach number of 2.62 compared with the nominal values of 1005 N/m^2 (21 lbf/ft^2) and 2.70. The density measurements that were used in the computer to predict the dynamic pressure were measured the day before the flight and were approximately 5 percent higher than the postflight measurements; therefore, 5 percent of the dynamic-pressure difference between actual and nominal values could be attributed to the difference in the density. The difference between the actual and nominal is about 6 percent and, considering the density difference and the error, shows that this computer method of obtaining the test point was quite satisfactory. The time history of dynamic pressure during the test period was presented in figure 21 and histories of velocity, Mach number, altitude, and flight-path angle were presented in figure 22. A cross plot of dynamic pressure and Mach number is presented in figure 26.

Starting at peak load, the parachute, which was in the wake of an oscillating blunt cone, oscillated violently and was extensively damaged. In spite of the damage, the parachute still retained 60 to 70 percent of its anticipated drag. The parachute data were obtained from the onboard cameras, tensiometers, and longitudinal accelerometers. The parachute data reduction and analysis is beyond the scope of this report and is presented in reference 6.

Seven seconds after the mortar fired, or at 247.2 seconds, the aeroshell separated from the payload-parachute. Observations from the forward-facing camera indicated that there was no damage to the aeroshell during the flight. The track of the aeroshell is shown in figure 13. In the absence of the aeroshell, the parachute still oscillated rather violently until the Mach number had decreased to about 1.5 when the oscillations were reduced considerably. When the payload-parachute had fallen to 4907 meters (16 100 ft) altitude, a third command was sent that released the ballast from the payload. The payload and parachute splashed in the water at 1655 seconds of flight time. This time was shorter than expected because of the decreased drag of the damaged parachute. The parachute and payload were recovered from the water for inspection and retrieval of the data film.

CONCLUDING REMARKS

A flight test of an expandable 4.57-meter-diameter (15-ft), 120° blunted-cone spacecraft configuration for testing large decelerators was conducted under simulated Mars entry conditions by using a ground-launched rocket vehicle to obtain the desired test conditions. A test parachute was deployed behind the blunted cone at a test condition of Mach number and dynamic pressure.

The test conditions desired for parachute deployment were a Mach number of 2.70 at a dynamic pressure of 1005 N/m^2 (21 lbf/ft^2). By use of a computer to calculate real-time dynamic pressure from radar tracking and premeasured density data, an estimation of when the test conditions would be met was obtained. A radio command sent to deploy the parachute resulted in a satisfactory test point. The test point obtained was a Mach number of 2.62 and a dynamic pressure of 929 N/m^2 (19.4 lbf/ft^2).

As the nose cone separated from the aeroshell, a disturbance caused the aeroshell to oscillate to a large amplitude. Postflight studies revealed that the wake of the separated nose cone and the large attitude angle at aeroshell erection did affect the aeroshell. Studies further indicated that this disturbance could be minimized by erecting the aeroshell and releasing the nose cone near zero dynamic pressure.

The dynamic stability parameters derived from six-degree-of-freedom simulations of the measured motions agreed well with referenced data. The measured drag coefficient of the aeroshell-payload combination agreed satisfactorily with preflight estimations.

Langley Research Center,
National Aeronautics and Space Administration,
Hampton, Va., August 29, 1972.

APPENDIX A

ATTITUDE CONTROL SYSTEM

By James C. Young
Langley Research Center

The overall objective of the attitude control system (ACS) is to orient the spacecraft to the proper attitude to insure a near-zero angle of attack at the time of aeroshell opening. The attitude control system accomplishes this by controlling the spacecraft to the proper attitude in roll, pitch, and yaw by use of a roll-stabilized attitude reference system and a cold-gas jet-reaction control system.

The attitude sensor consists of two single-degree-of-freedom gyros mounted on a roll-stabilized platform. One gyro has a readout in roll and yaw attitude, using the roll output to continually position the platform for roll stability, and the second gyro has a pitch attitude readout. These two gyros provide attitude information about the mutually orthogonal roll, pitch, and yaw axes of the spacecraft throughout the flight.

The attitude control system can be divided into two major parts, the despin system and the spacecraft control system.

The despin system is activated in the coast phase of the flight by a timer command (roll on) 30 to 35 seconds before the separation of the spacecraft from the booster. The controller part of the despin system consists of four reaction control jets located at the tip of the booster fins. (See fig. 5.) Three tanks, located in the interstage of the vehicle, contain 10.07 kg (22.2 lbm) of nitrogen at 2068 N/cm^2 (3000 psig) as fuel for the despin system. This nitrogen is supplied to the valves, located at the base of the fins, through 1.59-cm (5/8-in.) tubing in tunnels along each side of the booster. The reaction jets, operated in couples (one each way on the tips of opposing booster fins), produce a force of 37.8 N (8.5 lbf) per jet with 2068 N/cm^2 (3000 psig) pressure in the tanks. The force will decrease as the pressure decreases, as this is a nonregulated, or bleed-down, system.

Roll rates of up to 120 deg/sec from fin and thrust misalinements are possible during this phase of the flight. The despin system will reduce these rates to zero and then will orient the vehicle to a nominal zero roll condition. The despin system will hold this roll attitude until the separation of the booster from the spacecraft, at which time the reaction control jets located in the fins are no longer available.

The folded spacecraft configuration shown in figure 3(a) is aerodynamically unstable; therefore, it is necessary that the spacecraft be controlled in roll, pitch, and yaw. A single tank, containing 3.36 kg (7.4 lbm) of nitrogen at 2068 N/cm^2 (3000 psig) and

located in the nose cone of the spacecraft, supplies the nitrogen for all reaction control jets in the spacecraft control system. The 2068-N/cm^2 (3000-psig) nitrogen is regulated down to 420 N/cm^2 (610 psig) to produce 22.2 N (5 lbf) of force from each of the reaction control jets.

The roll of the spacecraft is controlled, after booster-spacecraft separation, by four 22.2-N (5-lbf) jets, operated in couples and located at the base of the nose cone of the spacecraft. (See fig. 3(a).)

The control law for the despin and the roll part of the spacecraft control system is a straight-line switching curve with a 10-deg/sec rate limit. The slope (position over rate) of this switching curve is 0.75. The position dead band is $\pm 2^{\circ}$ with a ±2.7-deg/sec rate dead band.

Very little difference exists between the pitch and yaw parts of the spacecraft control system; therefore, only the pitch part will be explained in full detail. The pitch control system is activated at the time of booster-spacecraft separation to control the aerodynamically unstable folded spacecraft.

As stated previously, the overall objective of the attitude control system is to provide a near-zero angle of attack at the time of aeroshell erection. The pitch angle required for this zero angle of attack is determined by the trajectory flown by the vehicle. The pitch angle is 180° minus the angle between the flight path and vertical at a predetermined time in the flight. It is assumed that the vehicle is alined with the flight path at this time. This angle (attitude reference) is recorded by the attitude control system at a command from the internal timer before booster-spacecraft separation for use later in the flight.

The vehicle is positioned on the launcher vertically with the underside facing the wind-corrected azimuth. This provides a zero reference because the gyro is uncaged with the vehicle in this position (vertical) and the launcher is then lowered to the wind-corrected launch elevation angle. The vehicle, after launch, will follow a predetermined trajectory, and the pitch angle will change as the vehicle moves along this trajectory. A follower servo is used to drive a reference potentiometer so that its output voltage will track the output of the pitch-control potentiometer. This follower servo is turned off at a predetermined time by a timer signal (attitude reference), and the reference potentiometer records the pitch angle at this time. This pitch angle is used as the reference attitude to which the spacecraft is oriented after the pitch reaction control jets are activated.

The pitch reaction control system is activated at booster-spacecraft separation. Two 22.2-N (5-lbf) pitch reaction control jets, located 49.17 cm (19.36 in.) from the theoretical tip of the 10° nose cone (fig. 3(a)), are used to control the folded spacecraft to the pitch attitude recorded at the time of the attitude reference command.

The pitch-over maneuver is necessary to insure a near-zero angle of attack in the pitch plane at aeroshell opening. The pitch maneuver is started at about 145 seconds by the pitch-over command from the internal timer. The spacecraft is being controlled to the attitude that was recorded by the reference potentiometer at attitude reference time. This reference attitude is changed from a pitch-up angle of some value to a pitch-down angle of the same value. This change is accomplished by reversing the excitation voltage on the reference potentiometer. The pitch electronics compare the output of the control potentiometer with the output of the reference potentiometer and fire the proper reaction jet to reorient the vehicle to the new pitch attitude. The pitch maneuver will move the vehicle about an axis that is perpendicular to the flight-path plane.

The pitch control law, like the roll control law, is based on a straight-line switching curve, with a 10-deg/sec rate limit. The slope (position over velocity) of the pitch switching curve is 0.667. The pitch dead band is $\pm 2^{\circ}$ with a rate dead band of ± 3 deg/sec.

The yaw control system is like the pitch control system and moves the vehicle in a plane perpendicular to the pitch plane. The yaw control law, dead bands, and reaction control jets are the same as those for the pitch control system. As stated in the text, the yaw control should be altered to not change the yaw attitude during the attitude maneuver in order to eliminate the large yaw angle that occurred in this flight.

The erection of the aeroshell (fig. 3(b)) makes the spacecraft an aerodynamically stable vehicle. The nose cone, with the nitrogen tanks and the reaction control jets, is ejected after aeroshell opening. This event ends the primary task of the attitude control system, which was to have a near-zero angle of attack at the time of aeroshell erection, and leaves only the task of attitude monitoring during the rest of the flight.

APPENDIX B

SIMULATION OF AEROSHELL MOTIONS DURING NOSE-CONE SEPARATION

A schematic depicting what is believed to have been the sequence of nose-cone separation from the erected aeroshell is presented in figure 27. The aeroshell experienced a severe angle-of-attack buildup (near 90^{o}) during the 1-second period following separation. It has been suggested that the unexpected aeroshell motions were induced by aerodynamic moments resulting from the aeroshell being in the wake of the separated nose cone. In order to determine the validity of this hypothesis, a simulation of the aeroshell motions in the oscillation plane during separation was conducted by utilizing the six-degree-of-freedom computer program described in reference 25. Aerodynamic force and moment coefficients input to the program were calculated from wind-tunnel data of reference 22. These wind-tunnel data have several limitations which may compromise the accuracy of the results. These limitations are as follows:

1. Reference length and area for force and moment calculations in the simulation were based on a 4.57-meter-diameter (15-ft) aeroshell, even though aerodynamic coefficients from reference 22 were based on an equivalent 3.5-meter-diameter (11.5-ft) aeroshell with the same size nose cone.

2. Wind-tunnel data were not obtained for the situation where the algebraic sign of nose-cone and aeroshell angle of attack are different; therefore, nose-cone angle of attack is assumed to be zero when its algebraic sign differs from that of the aeroshell.

3. Wind-tunnel data for position offsets of the nose cone with respect to the aeroshell normal to the velocity vector and in the plane of oscillation are available only for both bodies at zero angle of attack.

4. Wind-tunnel data were obtained for aeroshell angles of attack up to about 22^{o}, whereas the observed maximum angle of attack was near 90^{o}. Data at high angle of attack were estimated with no nose-cone wake effects considered.

Although these limitations make an exact simulation impossible, the magnitude of the angle of attack and the trend of the simulated aeroshell motion are reasonable.

The simulation result for flight time $225.179 \leq t \leq 226.8$ seconds is presented in figure 28. This figure compares the angle-of-attack history in the oscillation plane obtained from flight data with the simulated-angle-of-attack data. The effect of the nose-cone wake was in the direction to cause a negative pitching moment. In fact, the simulated-angle-of-attack history was even more severe than the flight data in that buildup was more rapid. Figure 28 also presents the results of a simulation with nose-cone separation at a dynamic pressure q of 24 N/m^2 (0.5 lbf/ft^2) (flight q at separation was about 192 N/m^2 (4.0 lbf/ft^2)). This simulation was conducted to demonstrate a

possible means of avoiding problems caused by nose-cone wake impingement on the aeroshell. Because of the lower dynamic pressure, the aeroshell motions induced by the aerodynamic moments are reduced to a more acceptable level.

On the basis of the simulation result in figure 28, it is concluded that the nose-cone wake acting on the trailing aeroshell was probably responsible for the high angles of attack observed on the flight.

REFERENCES

1. McFall, John C., Jr.; and Murrow, Harold N.: Parachute Testing at Altitudes Between 30 and 90 Kilometers. AIAA Aerodynamic Deceleration Systems Conference, Sept. 1966, pp. 116-121.

2. Whitlock, Charles H.; and Bendura, Richard J.: Inflation and Performance of Three Parachute Configurations From Supersonic Flight Tests in a Low-Density Environment. NASA TN D-5296, 1969.

3. Darnell, Wayne L.; Henning, Allen B.; and Lundstrom, Reginald R.: Flight Test of a 15-Foot-Diameter (4.6-Meter) 120° Conical Spacecraft Simulating Parachute Deployment in a Mars Atmosphere. NASA TN D-4266, 1967.

4. Lundstrom, Reginald R.; Darnell, Wayne L.; and Henning, Allen B.: Large-Scale Decelerator Flight Tests Simulating a Mars Environment. J. Spacecraft & Rockets, vol. 5, no. 9, Sept. 1968, pp. 1106-1108.

5. Brown, Clarence A., Jr.; Campbell, James F.; and Tudor, Dorothy H.: Experimental Wake Survey Behind a 120°-Included-Angle Cone at Angles of Attack of 0° and 5°, Mach Numbers From 1.60 to 3.95, and Longitudinal Stations Varying From 1.0 to 8.39 Body Diameters. NASA TM X-2139, 1971.

6. Eckstrom, Clinton V.; and Branscome, Darrell R. (With appendix B by Percy J. Bobbitt): High-Altitude Flight Test of a Disk-Gap-Band Parachute Deployed Behind a Bluff Body at a Mach Number of 2.69. NASA TM X-2671, 1972.

7. Stone, Irving: Atmosphere Data To Alter Voyager Design. Aviat. Week Space Technol., vol. 83, no. 21, Nov. 22, 1965, pp. 66-67, 69.

8. Preisser, John S.; and Murrow, Harold N.: A Method for Controlling Parachute Deployment Conditions in Simulated Planetary Environments. Proceedings of the Third National Conference on Aerospace Meteorology, Amer. Meterol. Soc., 1968, pp. 379-383.

9. Muraca, Ralph J.; and Hedgepeth, Kenneth D.: Gas-Powered Reentry Body Erection Mechanism. 6th Aerospace Mechanisms Symposium, George G. Herzl, ed., NASA TM X-2557, 1972, pp. 101-107.

10. Anon.: U.S. Standard Atmosphere, 1962. NASA, U.S. Air Force, and U.S. Weather Bur., Dec. 1962.

11. Muraca, Ralph J.: An Empirical Method for Determining Static Distributed Aerodynamic Loads on Axisymmetric Multistage Launch Vehicles. NASA TN D-3283, 1966.

12. Madden, Ragan B.: Computing Program for Axial Distribution of Aerodynamic Normal-Force Characteristics for Axisymmetric Multistage Launch Vehicles. NASA TN D-4342, 1968.

13. Suttles, John T.: Aerodynamic Characteristics From Mach 0.22 to 4.65 of a Two-Stage Rocket Vehicle Having an Unusual Nose Shape. NASA TN D-2163, 1964.

14. Martin, John C.; Margolis, Kenneth; and Jeffreys, Isabella: Calculations of Lift and Pitching Moments Due to Angle of Attack and Steady Pitching Velocity at Supersonic Speeds for Thin Sweptback Tapered Wings With Streamwise Tips and Supersonic Leading and Trailing Edges. NACA TN 2699, 1952.

15. Strass, H. Kurt, and Marley, Edward T.: Rolling Effectiveness of All-Movable Wings at Small Angles of Incidence at Mach Number From 0.6 to 1.6. NACA RM L51H03, 1951.

16. Brown, Clarence A., Jr.; and Carraway, Ausley B.: Static Aerodynamic Characteristics of a Two-Stage and a Three-Stage Rocket Vehicle at Mach Numbers From 1.47 to 4.63. NASA TN D-1232, 1962.

17. Henderson, James H.: Effect of Nose Bluntness on Normal Force, Pitching Moment, and Center of Pressure of Cone-Cylinder and Cone-Cylinder-Frustum Bodies of Revolution at Mach Numbers of 1.50, 2.18, 2.81, and 4.04. Rep. 6R11F, Ordnance Missile Labs., Redstone Arsenal, June 12, 1958.

18. Walker, Billy; and Weaver, Robert W.: Static Aerodynamic Characteristics of Blunted Cones in the Mach-Number Range From 2.2 to 9.5. Tech. Rep. 32-1213 (Contract No. NAS 7-100), Jet Propulsion Lab., California Inst. Technol., Dec. 1, 1967.

19. Marko, Wayne J.: Dynamic Stability of High-Drag Planetary Entry Vehicles at Transonic Speeds. J. Spacecraft, vol. 6, no. 12, Dec. 1969, pp. 1390-1396.

20. Hoerner, Sighard F.: Fluid-Dynamic Drag. Publ. by the author (148 Busteed Drive, Midland Park, New Jersey 07432), 1965.

21. Henning, Allen B.; Lundstrom, Reginald R.; and Keating, Jean C.: A Wind-Compensation Method and Results of Its Application to Flight Tests of Twelve Trailblazer Rocket Vehicles. NASA TN D-2053, 1964.

22. Brown, Clarence A., Jr.; Trescot, Charles D., Jr.; and Richardson, Celia S.: Experimental Aerodynamic Characteristics of 120°-Included-Angle Cone With Attached and Separated 20°-Included-Angle Cone at Mach Numbers of 2.36 and 2.70. NASA TM X-2603, 1972.

23. Preisser, John S.: Determination of Angles of Attack and Sideslip From Radar Data and a Roll-Stabilized Platform. NASA TM X-2514, 1972.

24. Uselton, B. L.; Shadow, T. O.; and Mansfield, A. C.: Damping-in-Pitch Derivatives of 120- and 140-Deg Blunted Cones at Mach Numbers From 0.6 Through 3. AEDC-TR-70-49, U.S. Air Force, Apr. 1970.

25. Dennison, A. J.; and Butler, J. F.: Missile and Satellite Systems Program for the I.B.M. 7090. Tech. Inform. Ser. No. 61 SD 170, Missile and Space Vehicle Dep., Gen. Elec. Co., Feb. 1962.

TABLE I.- ACCURACY[a]

Instrumentation:	
Yaw attitude, deg	±1.5
Pitch attitude, deg	±1.1
Roll attitude, deg	±4.5
Normal acceleration, g units	±0.1
Transverse acceleration, g units	±0.1
Longitudinal acceleration (low), g units	±0.1
Longitudinal acceleration (high), g units	±0.7
Velocity, m/sec (ft/sec)	±7.6 (±25)
Mach number	±0.03
Altitude, m (ft)	±30.4 (±100)
Horizontal range, m (ft)	±30.4 (±100)
Density, percent	±5
Dynamic pressure, percent	±5.3

[a]The estimated accuracies herein are especially applicable for an altitude range of 39.6 km (130 000 ft) to 57.9 km (190 000 ft).

TABLE II.- MASS CHARACTERISTICS OF VARIOUS CONFIGURATIONS

Configuration	Weight		Center of gravity		Roll moment of inertia		Pitch moment of inertia	
	kg	lbm	cm	in.	$kg\text{-}m^2$	$slug\text{-}ft^2$	$kg\text{-}m^2$	$slug\text{-}ft^2$
Flight:								
Total vehicle at launch	6688.3	14 745.2	707.49	278.54	783.5	577.9	49 949.0	36 840.5
Total vehicle at burnout	3076.8	6 783.2	586.54	230.92	426.1	314.3	33 932.5	25 027.3
Spacecraft (aeroshell closed)	1389.0	3 062.2	296.16	116.60	82.3	60.7	999.1	736.9
Spacecraft (aeroshell opened)	1389.0	3 062.2	283.00	111.42	714.2	526.8	1 199.1	884.4
Aeroshell-payload (before parachute deployment)	1196.0	2 636.7	302.00	118.90	704.5	519.6	831.6	613.4
Aeroshell-payload (without parachute system and sabot)	1136.2	2 505.0	296.47	116.72	704.1	519.3	758.6	559.5
Aeroshell-payload-parachute system	1193.5	2 631.2	-----	-----	----	----	-------	-------
Payload with ballast	610.5	1 346.0	320.78	126.29	21.3	15.7	203.1	149.8
Payload without ballast	257.6	568.0	373.86	147.19	14.5	10.7	68.7	50.7
Payload-parachute system with ballast	667.8	1 472.2	-----	-----	----	----	-------	-------
Payload-parachute system without ballast	314.9	694.2	-----	-----	----	----	-------	-------
Miscellaneous:								
Booster stage alone (loaded)	5300.4	11 683.1	815.29	320.98	701.2	517.2	19 292.3	14 229.3
Booster stage alone (empty)	1687.9	3 721.1	825.45	324.98	343.8	253.6	11 587.5	8 546.5
Nose cone alone	193.0	425.4	165.30	65.08	9.8	7.2	60.2	44.4
Aeroshell alone	525.7	1 159.0	268.22	105.60	682.7	503.5	477.4	352.1
Ballast and ballast clamp	352.9	778.0	282.04	111.04	6.8	5.0	8.8	6.5
Parachute, bag, risers, and mortar cover (packed)	57.2	126.2	408.61	160.87	.4	.3	2.7	2.0
Parachute, bag, risers, and mortar cover (deployed)	57.2	126.2	-----	-----	----	----	-------	-------
Sabot	2.5	5.5	385.65	151.83	----	----	-------	-------

TABLE III.- MASS CHARACTERISTICS DURING THRUST

Time, sec	Weight		Center of gravity		Roll moment of inertia		Pitch moment of inertia	
	kg	lbm	cm	in.	kg-m^2	slug-ft^2	kg-m^2	slug-ft^2
0	6688.3	14 745.2	707.49	278.54	783.5	577.9	49 949.0	36 840.5
.5	6573.1	14 491.2	703.91	277.13	765.1	564.3	49 176.7	36 270.9
1.0	6457.4	14 236.2	700.18	275.66	747.5	551.3	48 387.8	35 689.0
1.5	6342.7	13 983.2	696.34	274.15	728.5	537.3	47 585.4	35 097.2
1.8	6279.2	13 843.2	694.23	273.32	716.3	528.3	47 151.8	34 777.4
2.0	6242.4	13 762.2	693.17	272.90	712.2	525.3	46 927.3	34 611.8
2.2	6209.3	13 689.2	692.18	272.51	708.1	522.3	46 733.9	34 469.2
2.4	6180.7	13 626.2	691.41	272.21	704.1	519.3	46 593.9	34 365.9
4.0	6004.7	13 238.2	688.44	271.04	700.0	516.3	46 046.7	33 962.3
8.0	5563.9	12 266.2	679.96	267.70	679.7	501.3	44 630.3	32 917.6
12.0	5123.4	11 295.2	670.03	263.79	649.8	479.3	43 130.2	31 811.2
16.0	4683.0	10 324.2	658.22	259.14	613.2	452.3	41 517.7	30 621.9
20.0	4242.5	9 353.2	643.97	253.53	568.5	419.3	39 775.5	29 336.9
24.0	3801.6	8 381.2	626.39	246.61	511.5	377.3	37 861.6	27 925.3
27.3	3438.3	7 580.2	608.53	239.58	468.2	345.3	36 144.9	26 659.1
30.0	3216.1	7 090.2	595.60	234.49	446.5	329.3	34 971.7	25 793.8
32.0	3134.9	6 911.2	590.42	232.45	439.7	324.3	34 441.8	25 403.0
34.0	3104.0	6 843.2	588.39	231.65	432.9	319.3	34 151.4	25 188.8
36.0	3089.1	6 810.2	587.38	231.25	428.8	316.3	34 002.5	25 079.0
38.0	3083.2	6 797.2	586.97	231.09	427.5	315.3	33 967.6	25 053.2
40.3	3076.8	6 783.2	586.54	230.92	426.1	314.3	33 932.5	25 027.3

TABLE IV.- AERODYNAMIC CHARACTERISTICS

(a) Total vehicle

[C_m reference is the fin center line; x_{cg} and x_{cp} measured from apex of 10° nose cone; S = 0.0929 m^2 (1.0 ft^2), d = 0.3048 m (1.0 ft)]

M	C_{N_α}	C_{m_α}	x_{cp}		C_{m_q}	C_{l_δ}	C_{l_p}
			m	ft			
0	135.78	366.93	10.04	33.01	-40 534	407	-2650
.2	138.02	366.93	10.06	33.05	-42 413	413	-2665
.5	144.41	355.93	10.12	33.25	-47 262	434	-2825
.8	154.79	346.77	10.18	33.47	-52 464	491	-3190
1.0	187.48	394.46	10.23	33.61	-65 041	600	-3900
1.2	191.46	413.17	10.21	33.55	-67 954	615	-4000
1.5	135.57	442.09	9.87	32.45	-48 868	420	-2590
2.0	99.10	438.88	9.52	31.29	-36 732	286	-1830
2.5	79.85	490.24	8.99	29.54	-29 924	216	-1420
3.0	69.40	489.36	8.72	28.66	-26 854	170	-1150
3.5	62.59	486.13	8.50	27.93	-25 561	143	-975
4.0	57.24	485.76	8.23	27.21	-24 726	130	-865
4.5	54.65	486.43	8.16	26.81	-24 613	125	-810
5.0	52.53	487.57	8.04	26.43	-24 239	122	-790

(b) Folded spacecraft

[x_{cg} and x_{cp} measured from apex of 10° nose cone; C_N based on body cross-sectional area of 0.4870 m^2 (5.241 ft^2)]

α, deg	x_{cp} for M = 2.18 to 4.04		C_N	
	m	ft	M = 2.18	M = 4.04
0	1.98	6.5	0	0
2	2.01	6.6	.106	.106
4	2.06	6.78	.235	.235
6	2.14	7.02	.346	.346
8	2.23	7.34	.490	.473
10	2.34	7.70	.640	.612
12	2.40	7.88	.826	.761
15	2.45	8.04	1.150	1.000
20	2.51	8.26	2.025	1.570
30	2.61	8.57	3.040	2.360
40	2.67	8.77	4.050	3.140
60	2.71	8.90	5.700	4.530

(c) Erected aeroshell

[C_m reference is c.g. $\left(\frac{x_{cg}}{d} = 0.222\right)$; x_{cg} and x_{cp} measured from apex of 120° cone; all coefficients based on cone diameter of 4.572 m (15.00 ft) and cross-sectional area of 16.42 m^2 (176.7 ft^2)]

α, deg	M = 2					M = 3					M = 4				
	C_N	C_X	C_{m_q}	x_{cp}		C_N	C_X	C_{m_q}	x_{cp}		C_N	C_X	C_{m_q}	x_{cp}	
				m	ft				m	ft				m	ft
0	0	1.590	-0.20	3.58	11.78	0	1.567	-0.20	3.43	11.28	0	1.534	-0.20	3.28	10.79
5	.021	1.580	-.20	3.58	11.78	.022	1.558	-.20	3.43	11.28	.023	1.520	-.20	3.28	10.79
10	.042	1.563	-.20	3.58	11.78	.046	1.520	-.20	3.28	10.78	.048	1.480	-.20	3.14	10.33
15	.060	1.532	-.20	3.53	11.60	.074	1.460	-.20	3.26	10.70	.080	1.408	-.20	3.19	10.47
20	.082	1.486	-.20	3.34	10.97	.103	1.380	-.20	3.34	10.99	.115	1.310	-.20	3.23	10.63
25	.106	1.424	-.20	3.41	11.22	.132	1.277	-.20	3.39	11.14	.148	1.210	-.20	3.32	10.90

TABLE V.- SEQUENCE OF EVENTS FOR NOMINAL AND ACTUAL TRAJECTORY

Event	Time, sec		Mach number		Dynamic pressure				Altitude			
	Nominal	Actual	Nominal	Actual	Nominal		Actual		Nominal		Actual	
					N/m^2	lbf/ft^2	N/m^2	lbf/ft^2	m	ft	m	ft
Booster burnout	40.3	-------	4.06	----	20 646	431.2	----	-----	27 329	89 663	------	-------
Start roll capture	60.0	60.15	3.15	2.99	800	16.7	1044	21.8	47 220	154 922	44 457	145 857
Vehicle attitude sampling	79.0	79.03	2.78	2.53	81	1.7	115	2.4	62 843	206 177	58 977	193 494
Booster-spacecraft separation	90.0	90.08	2.67	2.37	24	.5	38	.8	70 290	230 609	65 800	215 881
Start entry attitude manuever	145.0	144.99	1.84	1.70	.5	.01	1	.02	90 188	295 894	82 692	271 300
Aeroshell erection	220.0	224.50	2.65	2.59	24	.5	176	3.68	71 087	233 226	56 314	184 758
Mortar fires	256.5	240.31	2.73	2.69	910	19.0	873	18.24	43 785	143 651	44 300	145 343
Test conditions (parachute peak load)	257.7	241.53	2.70	2.62	1 005	21.0	931	19.45	42 841	140 556	43 360	142 256
Aeroshell-payload separation	263.7	247.23	1.55	1.84	541	11.3	749	15.64	39 223	128 686	39 678	130 177
Ballast release	1291.0	1099.40	.04	.04	62	1.3	57	1.2	4 572	15 000	4 906	16 095
Splashdown	1884.0	1655.00	.02	----	29	.6	----	-----	0	0	0	0

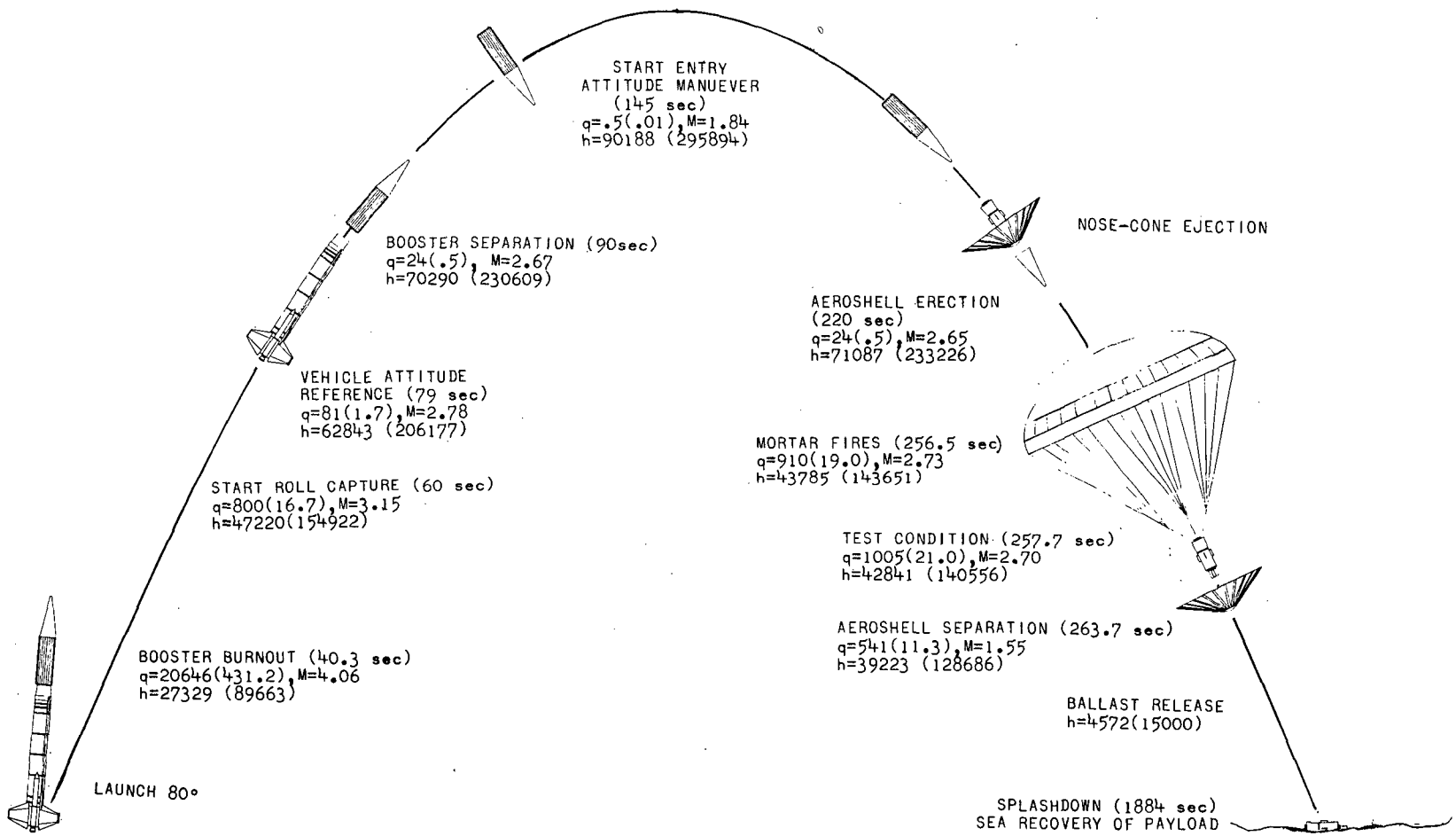

Figure 1.- Illustration of sequence of events of nominal trajectory. Altitudes are given in meters (feet), dynamic pressures in newtons/meter^2 (pounds-force/foot^2).

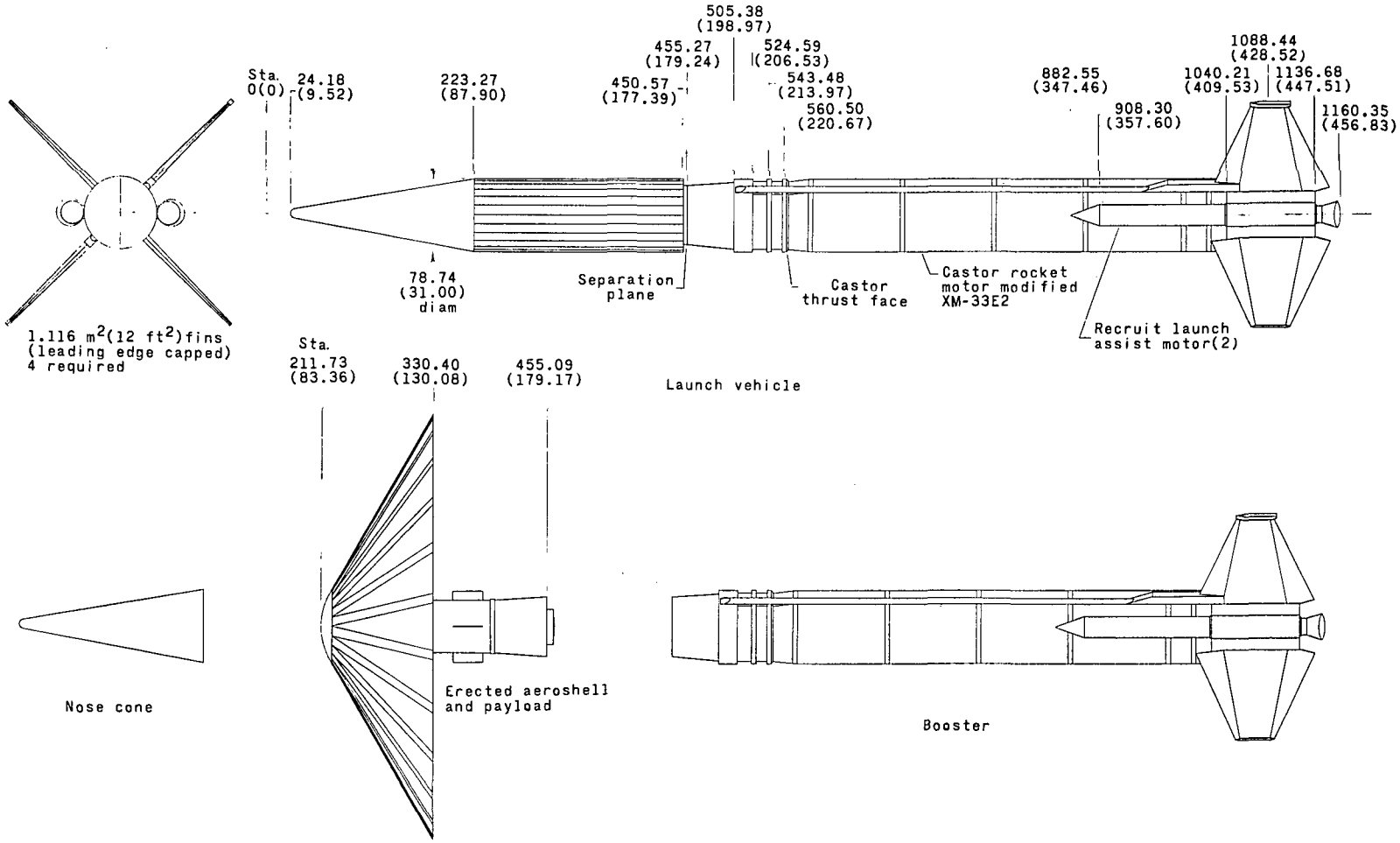

Figure 2.- Sketch of launch vehicle and separated parts including erected aeroshell and payload. All station numbers and dimensions are in centimeters (inches).

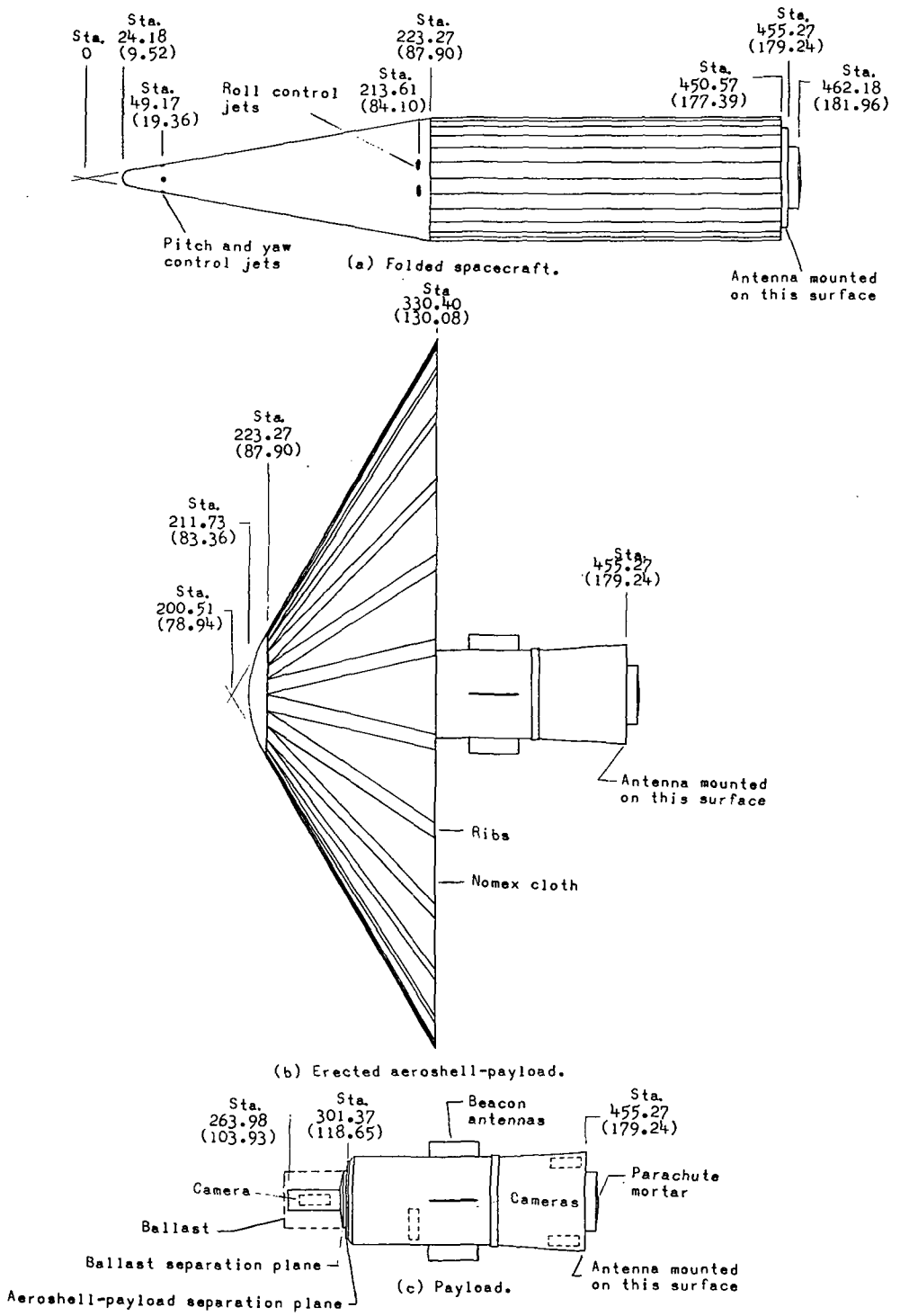

Figure 3.- Sketch of folded aeroshell, erected aeroshell-payload, and payload alone. All station numbers and dimensions are in centimeters (inches).

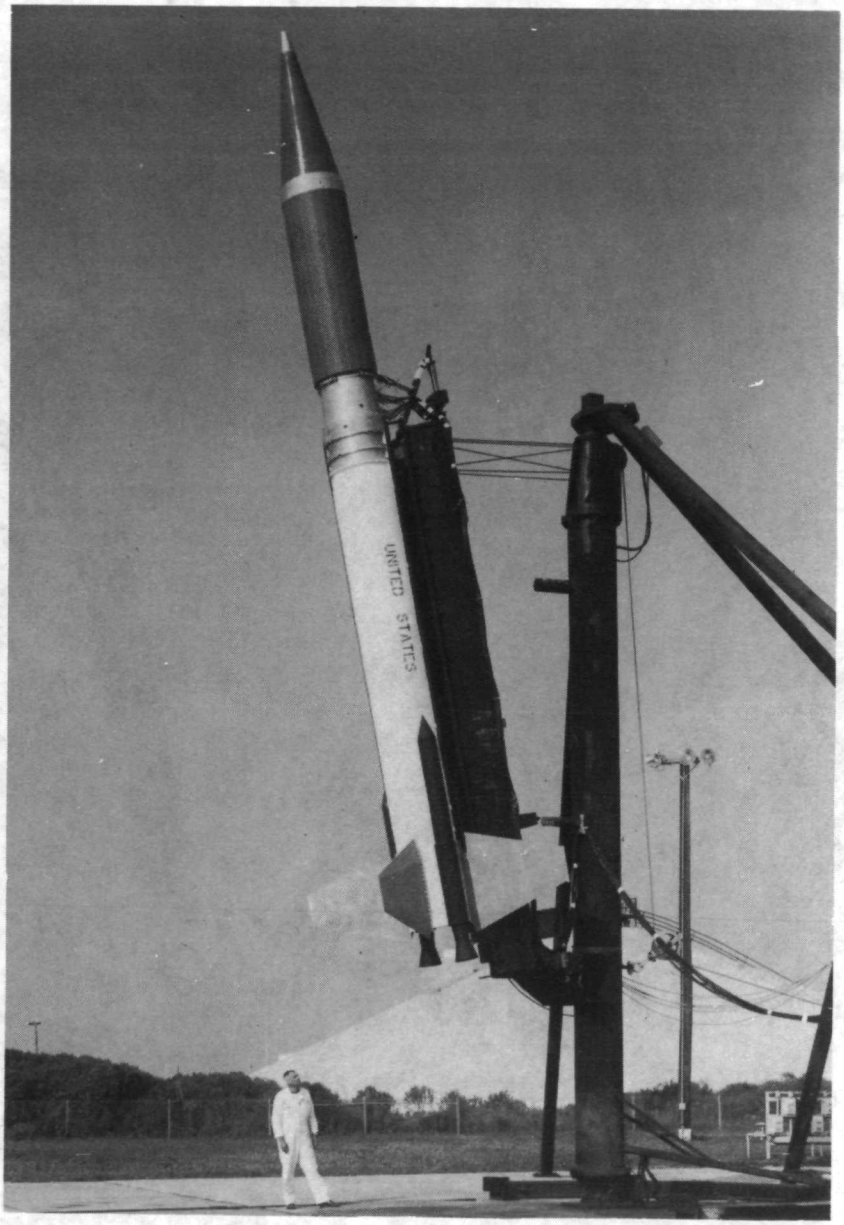

L-70-258

Figure 4.- Test vehicle on launcher.

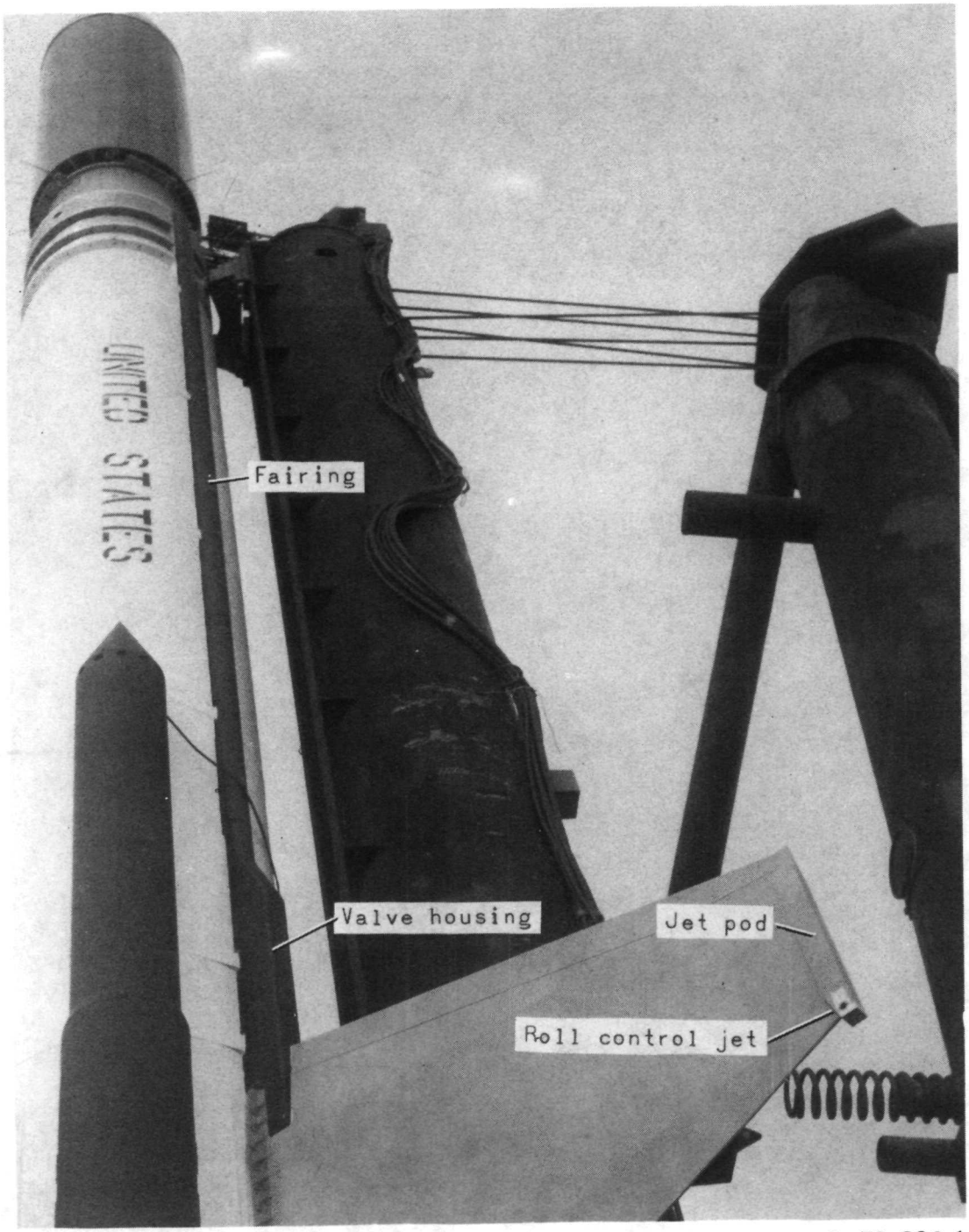

L-70-286.1

Figure 5.- Detail of roll control jets, jet pod, valve housing, and fairing of despin system.

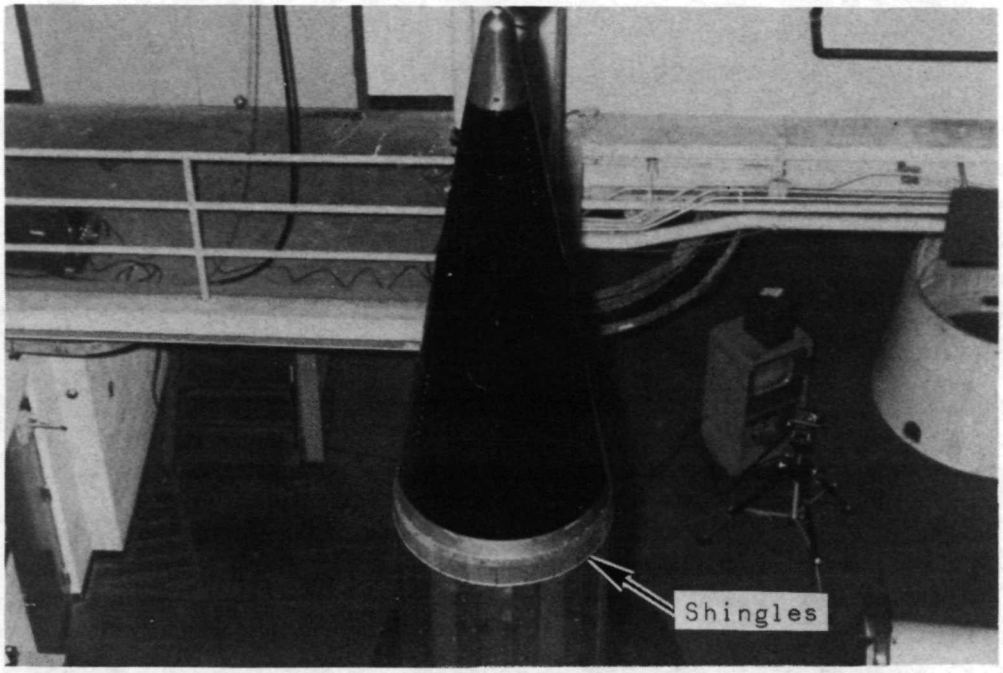

L-69-6725.1

(a) Folded aeroshell.

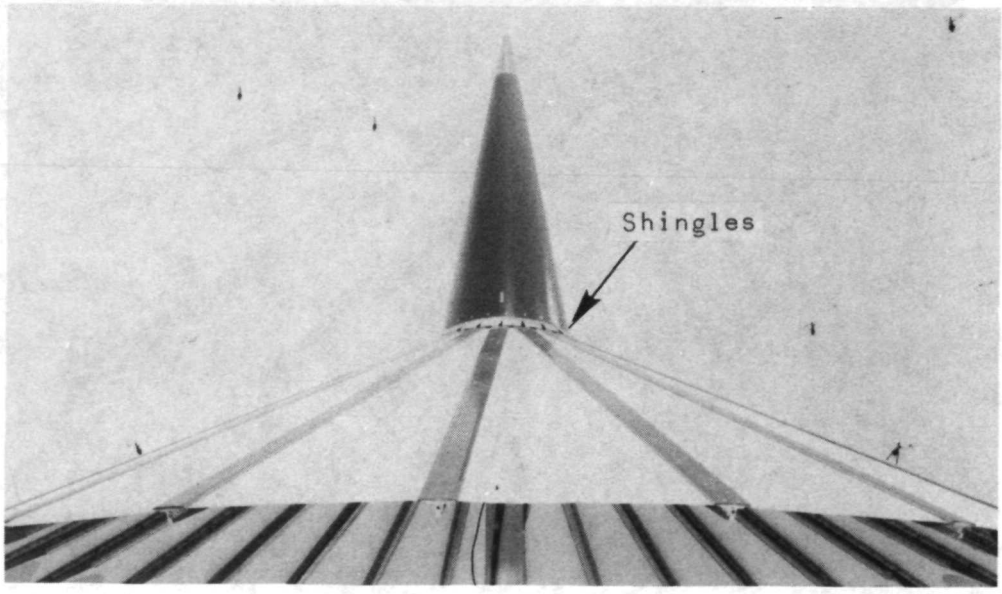

L-68-1923.1

(b) Opened aeroshell.

Figure 6.- Shingles over cone-cylinder juncture.

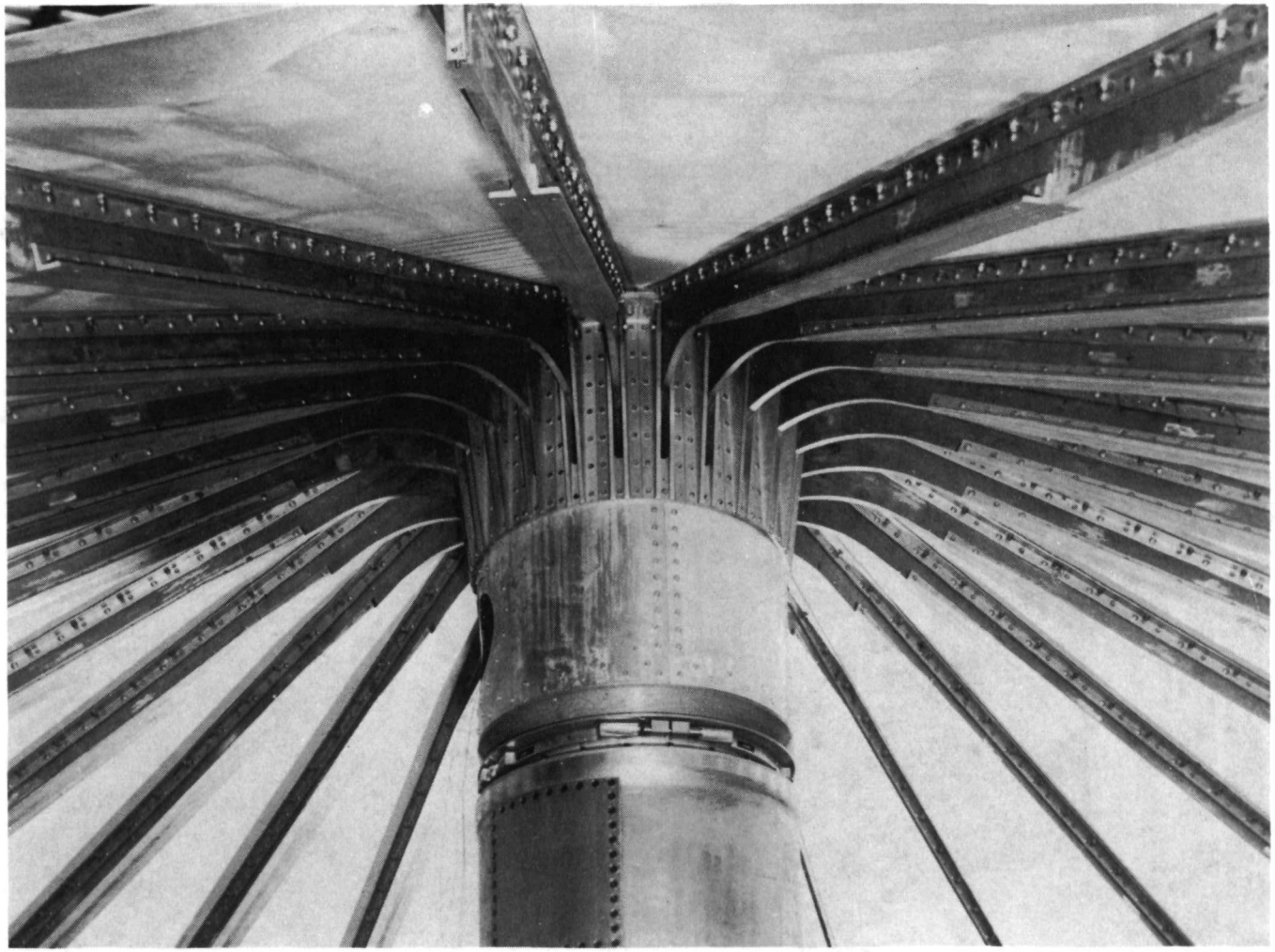

L-69-2143

Figure 7.- Aeroshell ribs mounted in central hub.

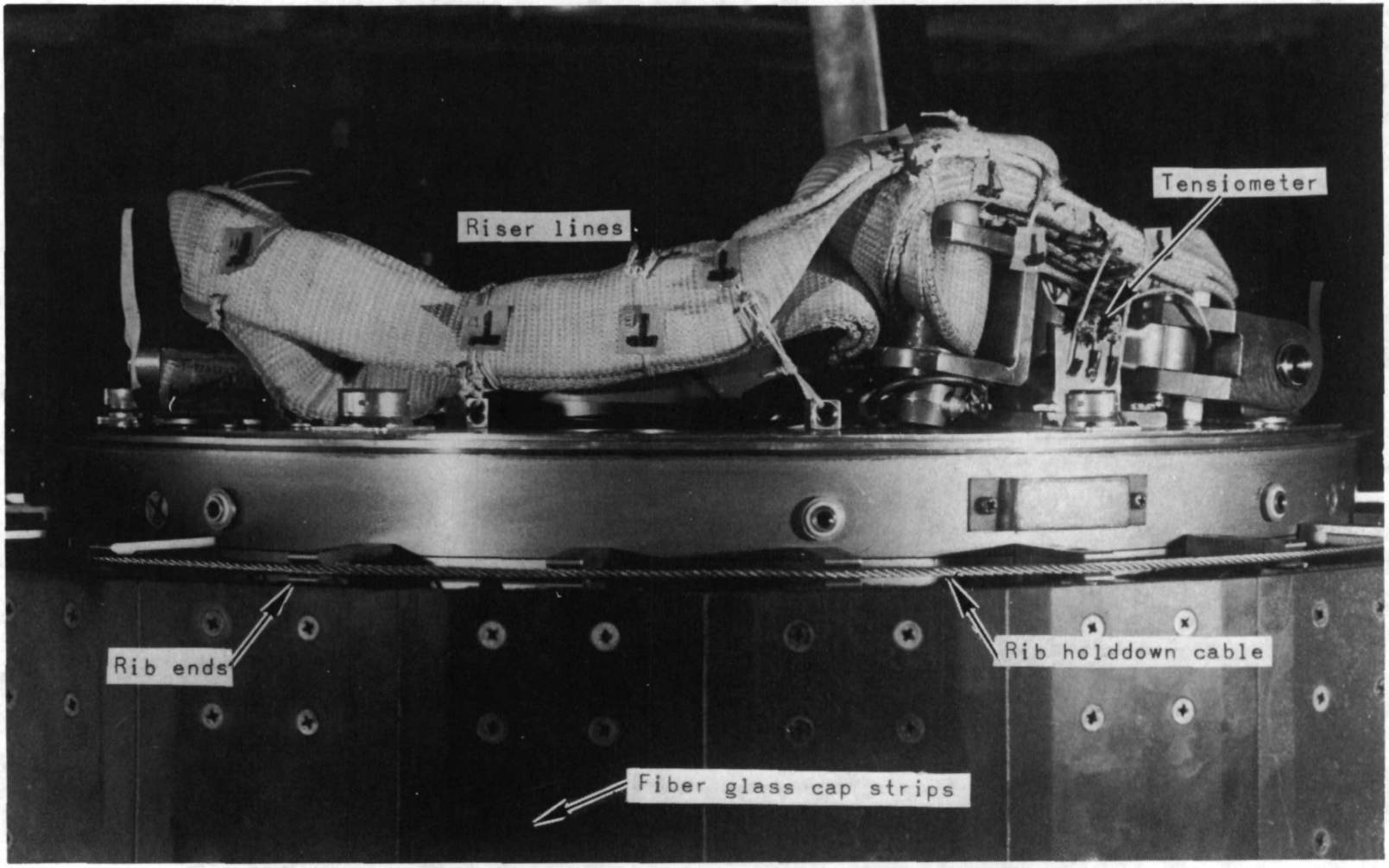

L-69-6764.1

Figure 8.- Aft end of folded aeroshell showing rib ends, fiber glass cap strips, rib holddown cable, tensiometers, and folded riser lines.

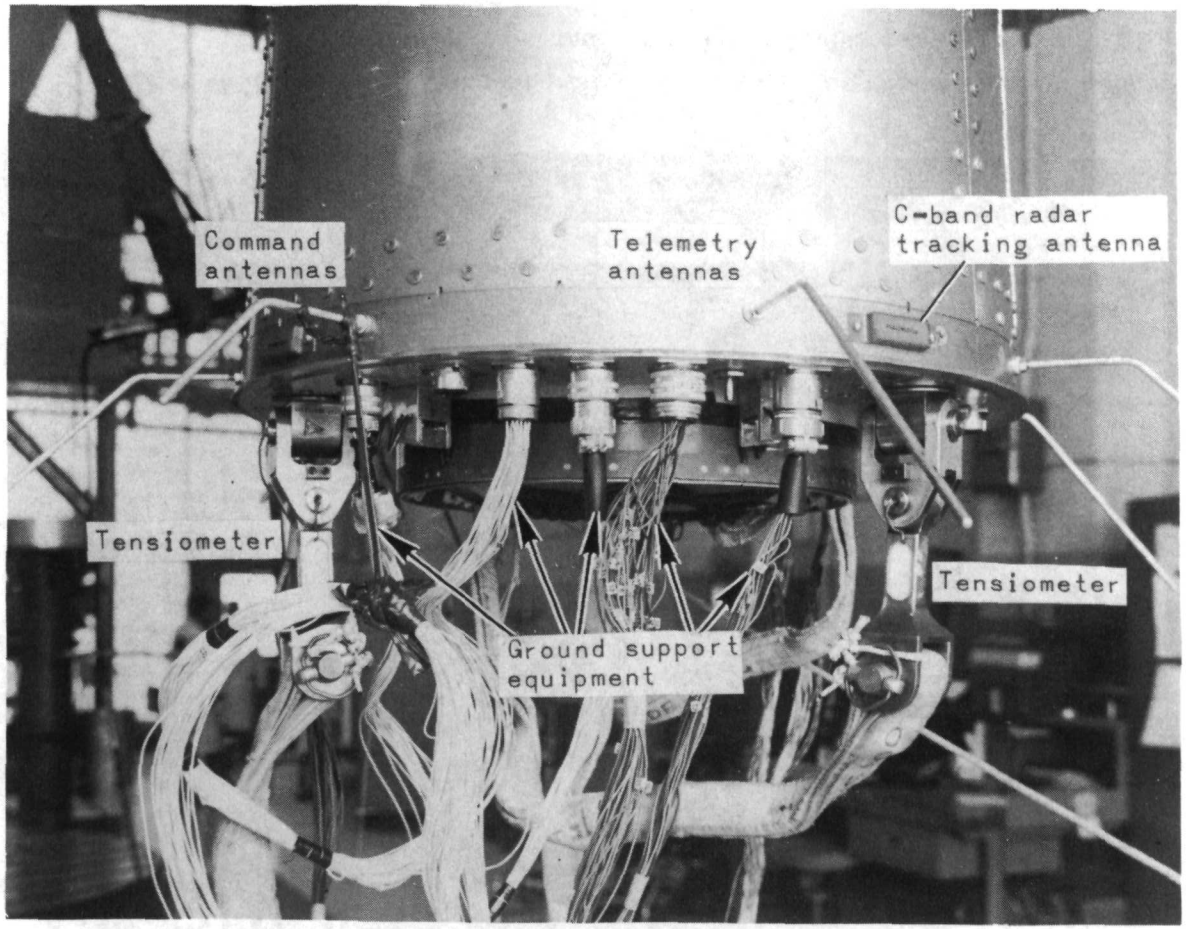

L-70-21.1

Figure 9.- Aft end of payload showing antennas and extended tensiometers.

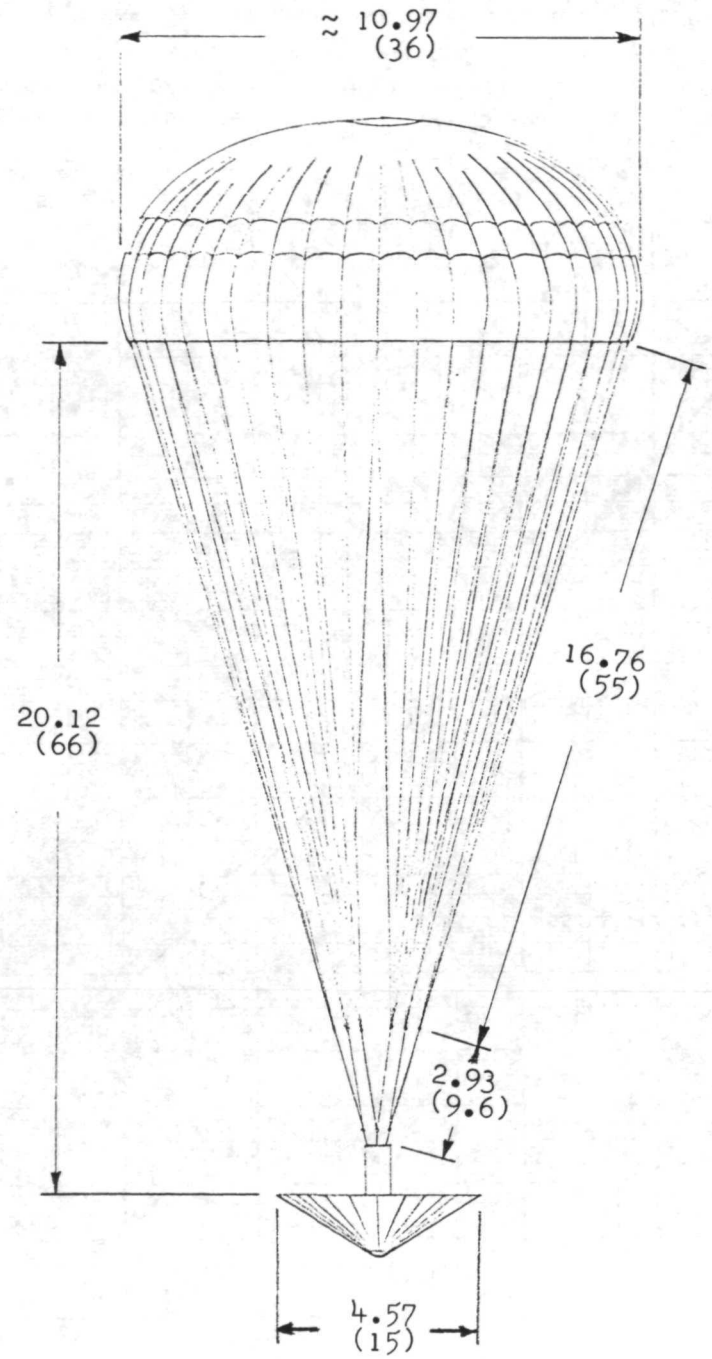

Figure 10.- Sketch of parachute-payload system with aeroshell.
All dimensions are in meters (feet) unless otherwise noted.

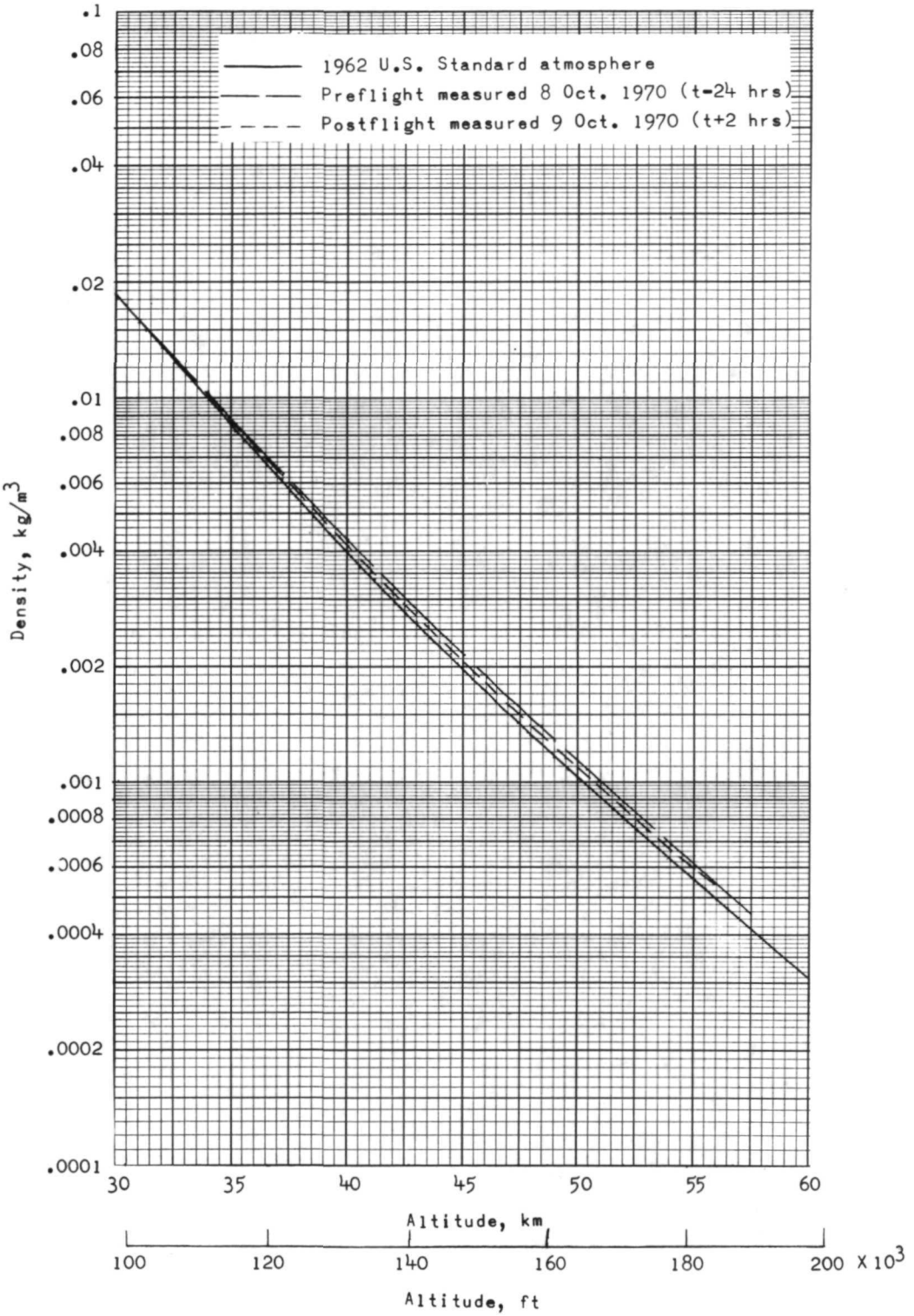

Figure 11.- Variation of atmospheric density with altitude. (To obtain density in lbm/ft^3, multiply value in kg/m^3 by 0.062.)

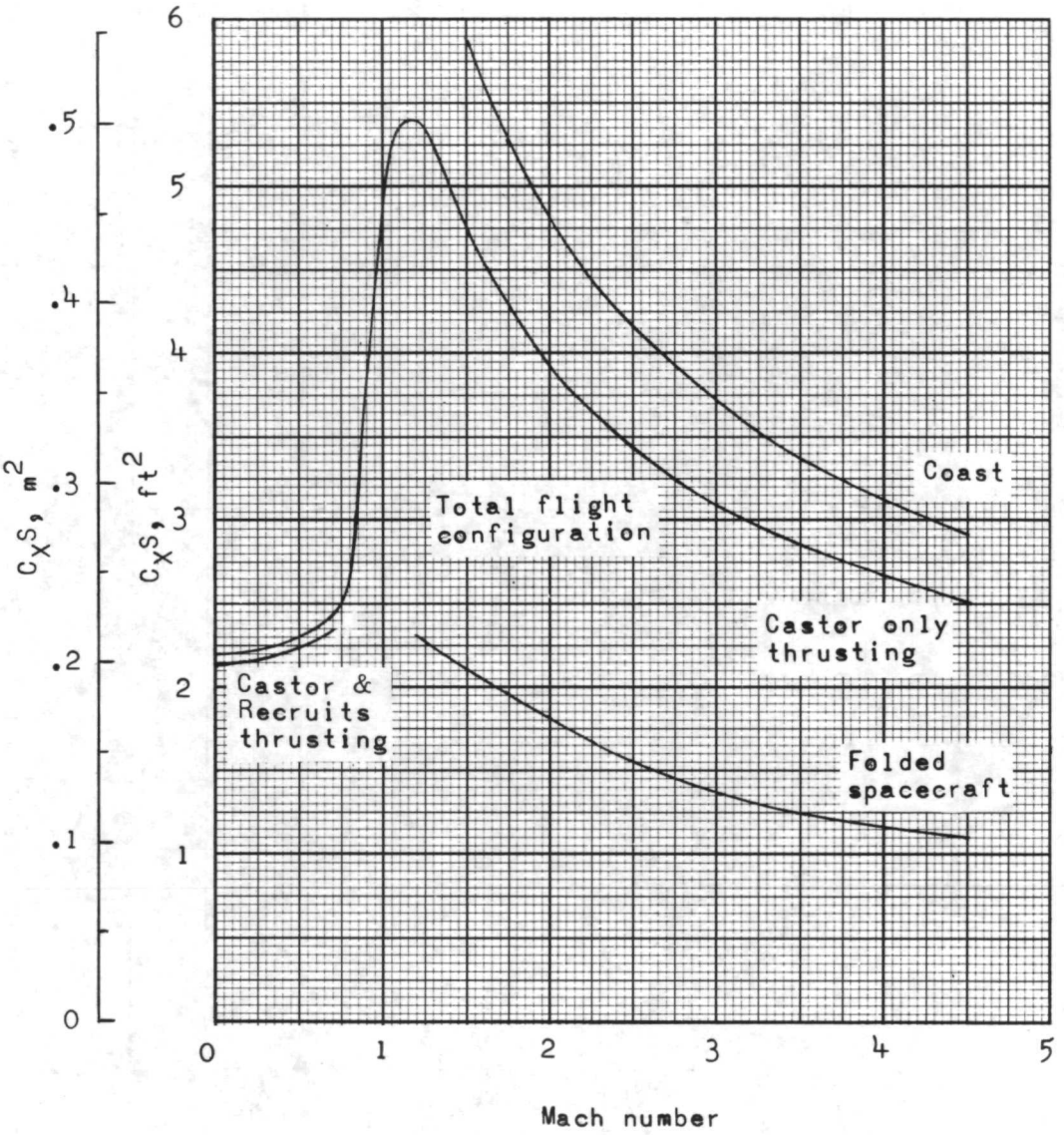

Figure 12.- Variation of axial-force coefficient with Mach number of total flight configuration during various flight conditions and of folded spacecraft. S = 0.0929 m^2 (1 ft^2).

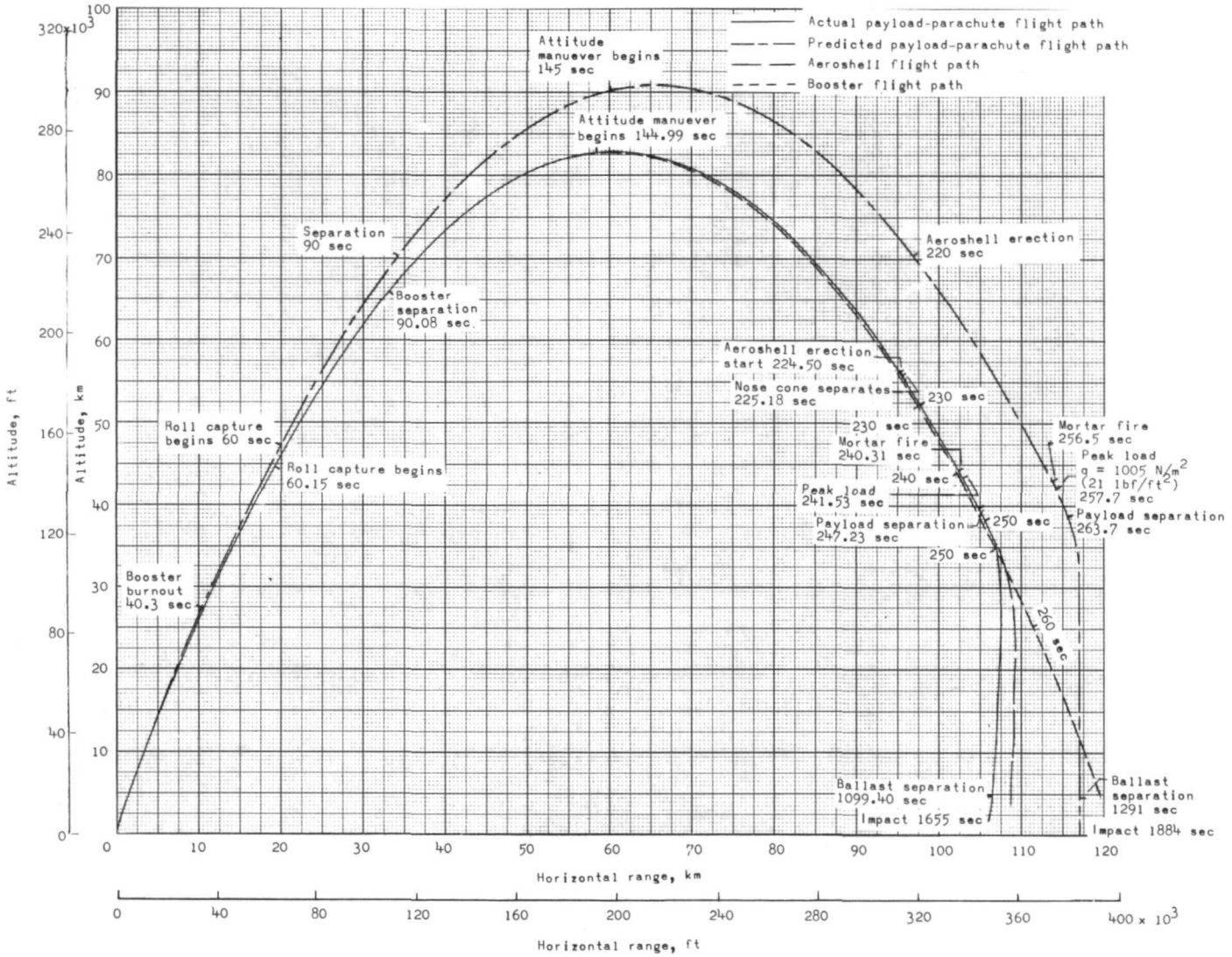

Figure 13.- Variation of altitude with horizontal range of nominal and flight trajectories of complete parachute-payload with event times. Included are aeroshell and booster flight trajectories.

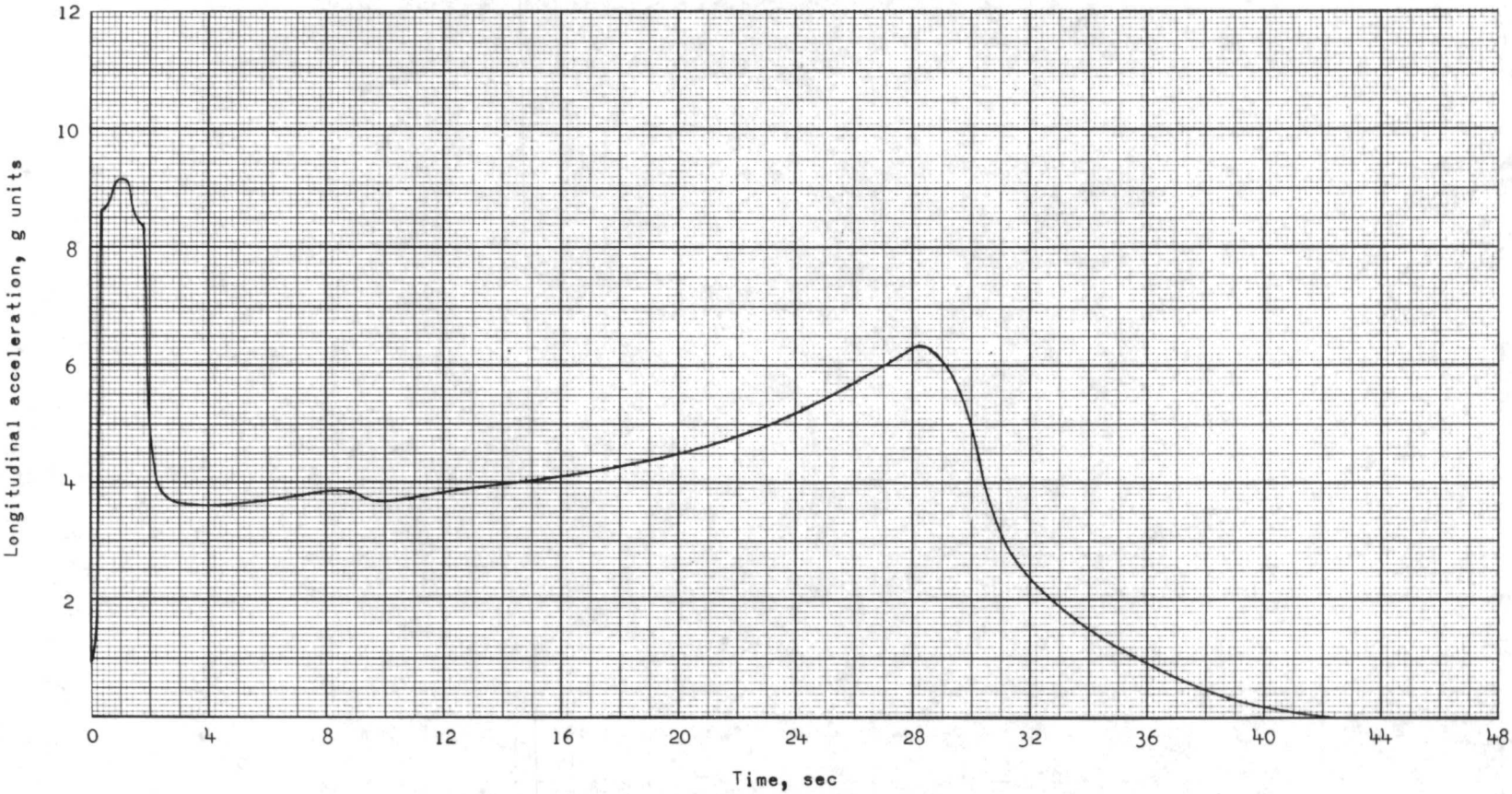

Figure 14.- Variation of acceleration with time during thrust.

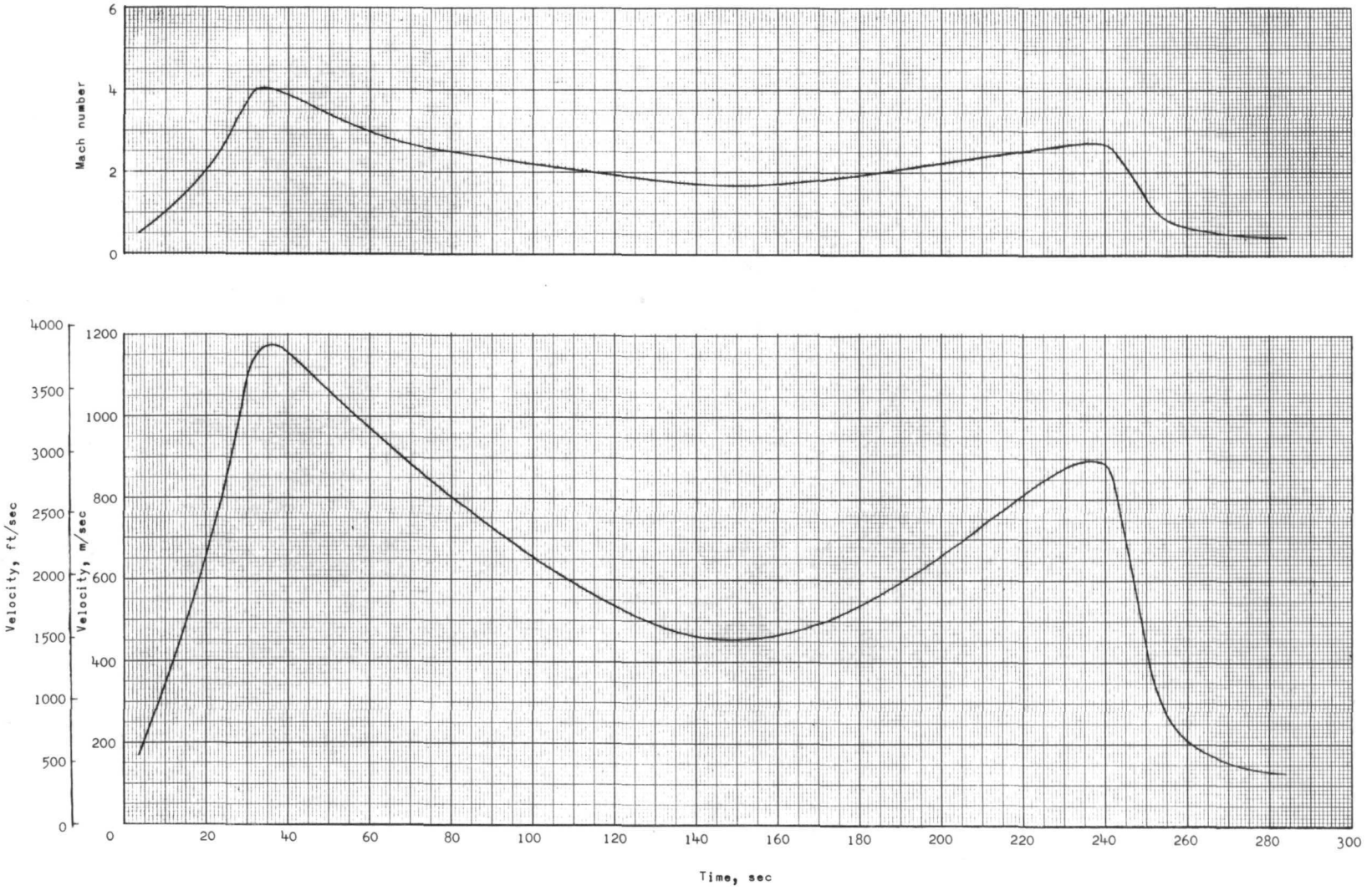

Figure 15.- Variation of velocity and Mach number with time.

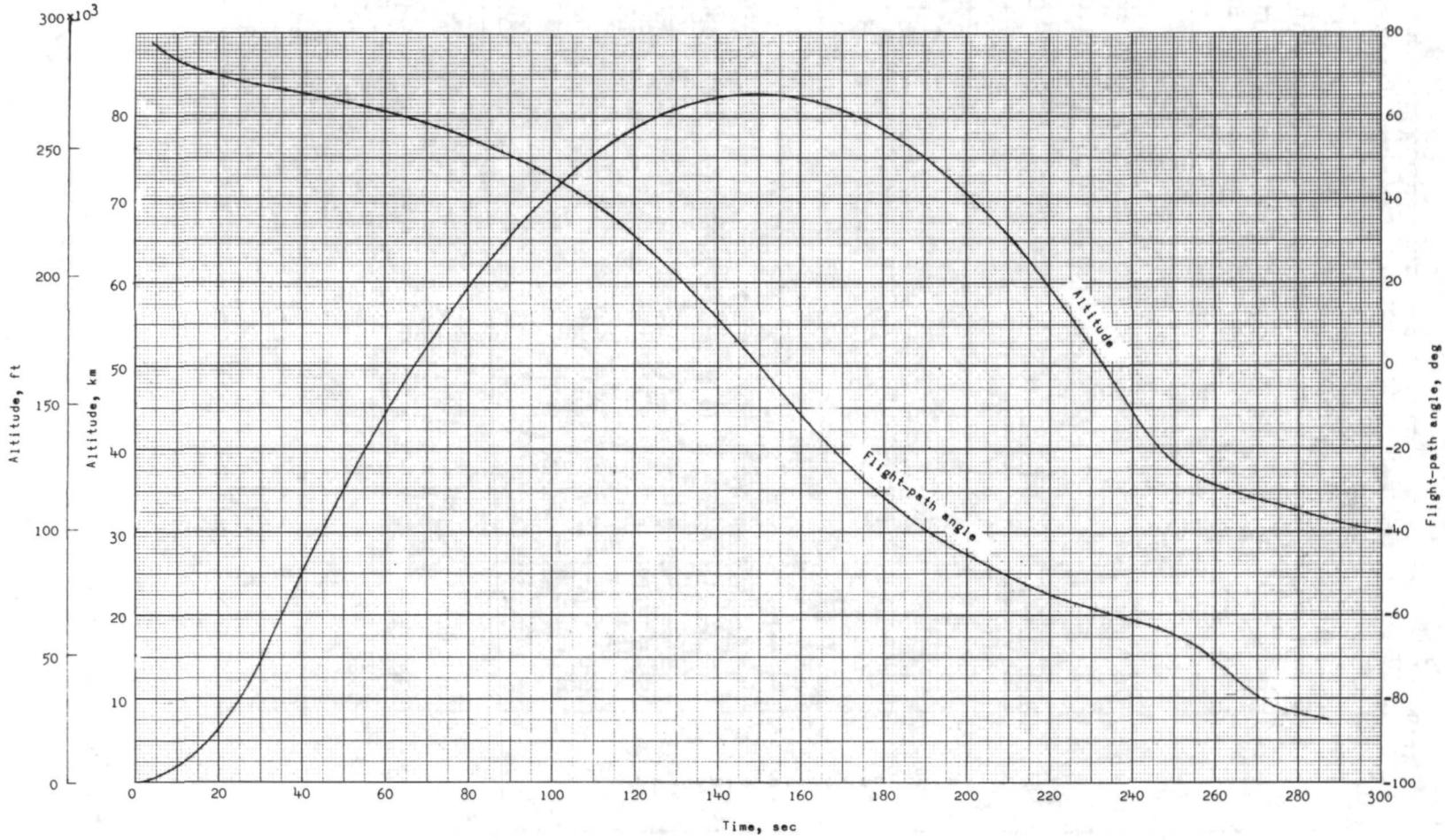

Figure 16.- Variation of altitude and flight-path angle with time.

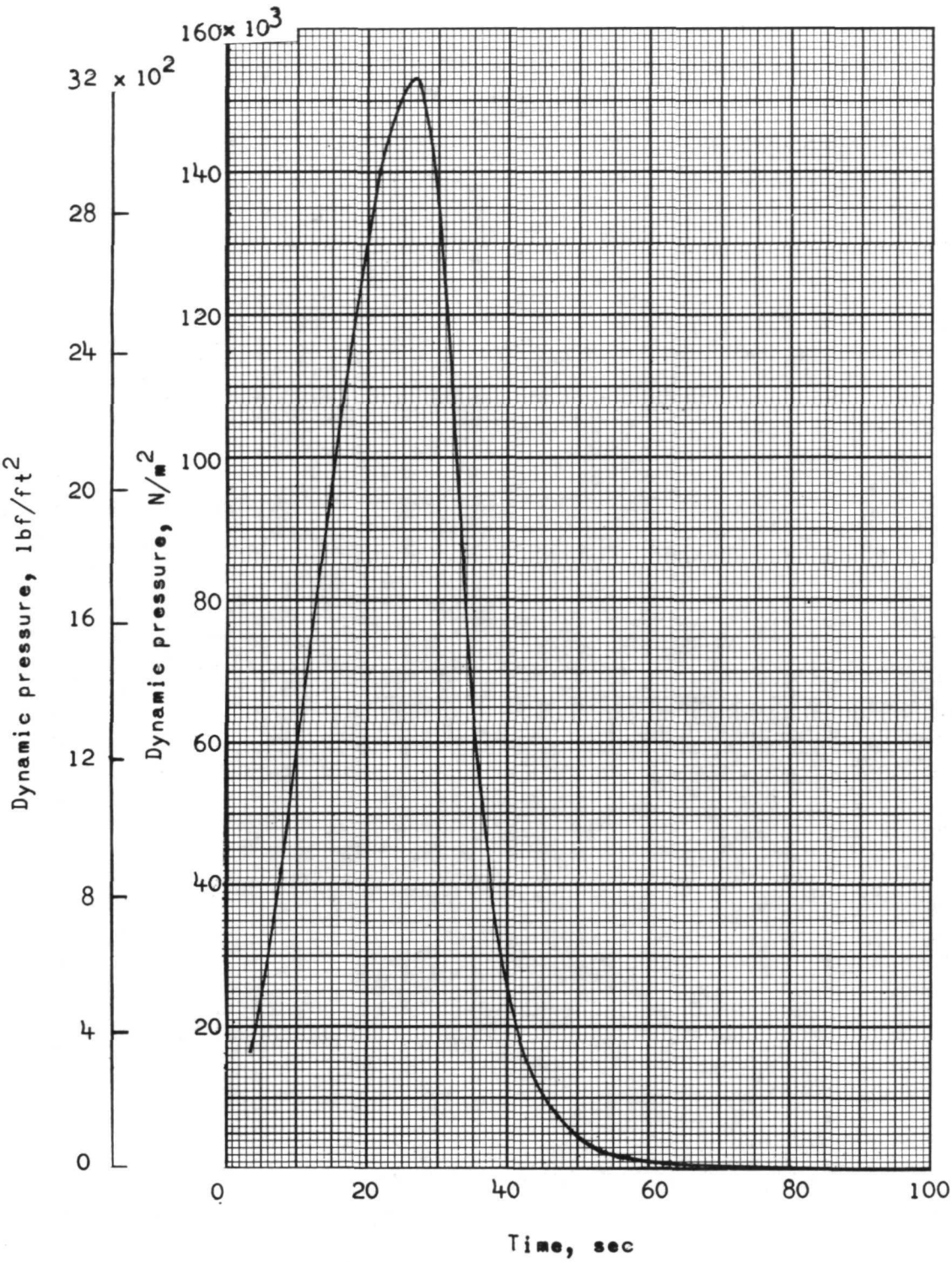

Figure 17.- Variation of dynamic pressure with time before booster-spacecraft separation.

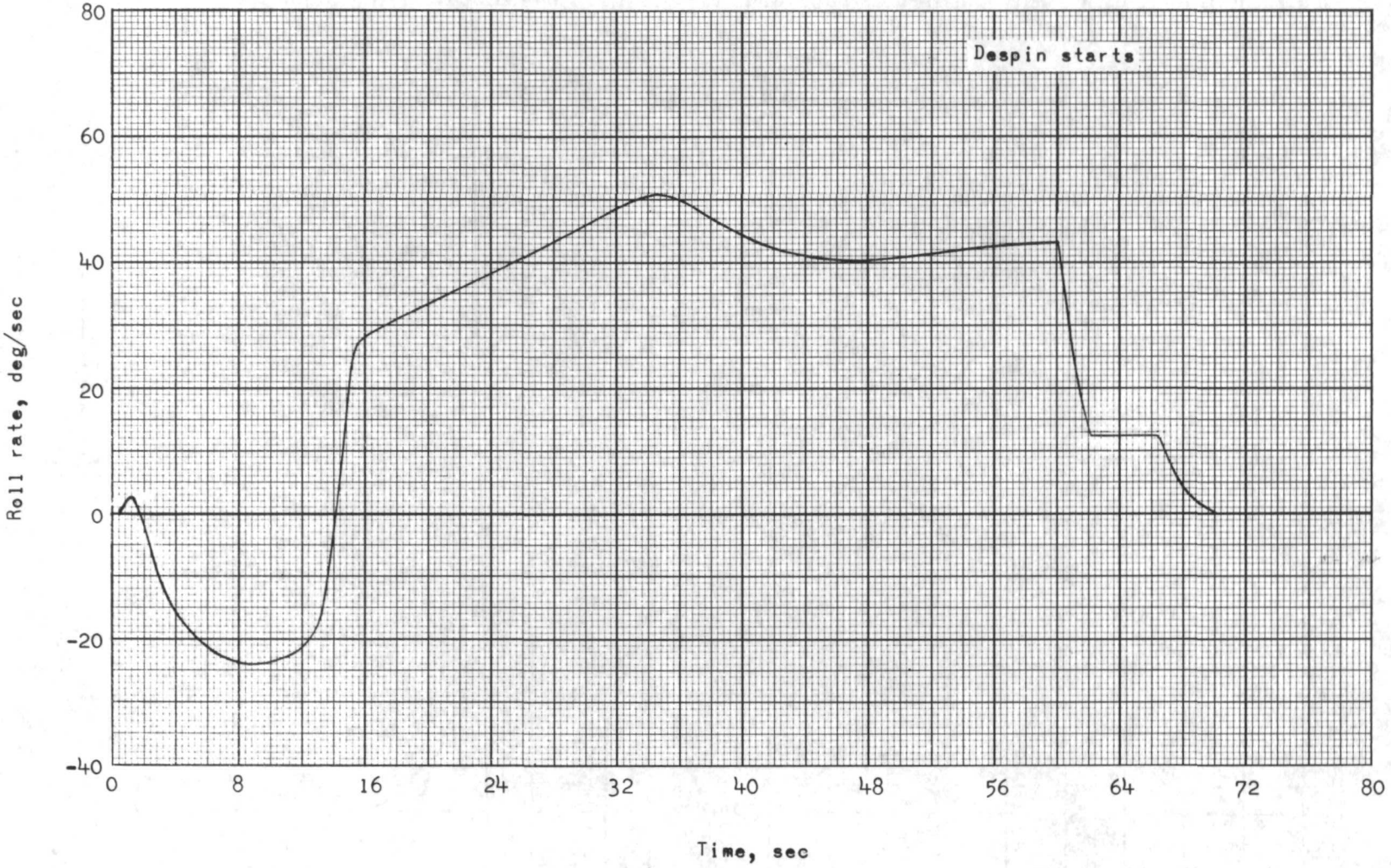

Figure 18.- Variation of roll rate with time during and after thrust.

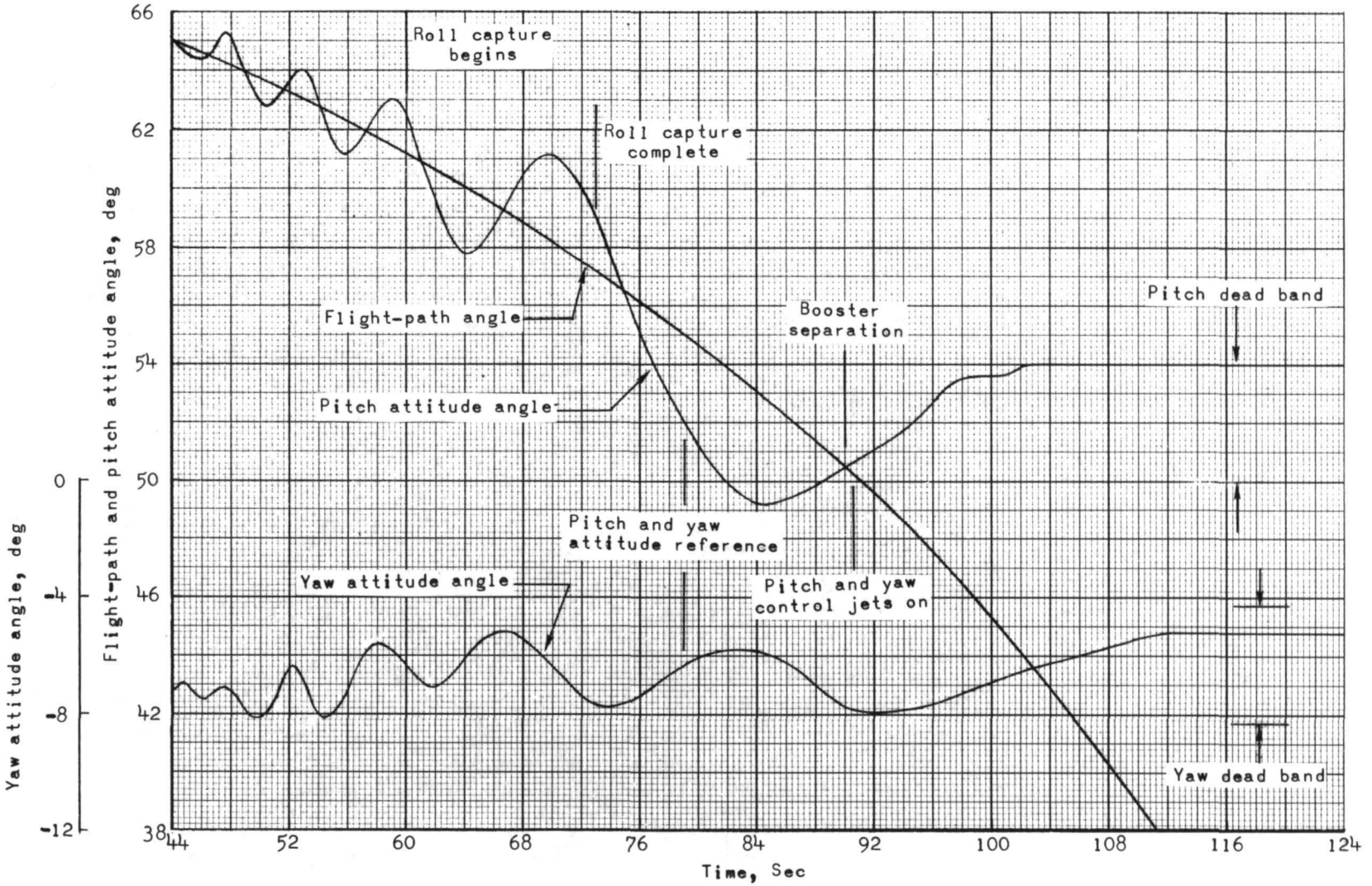

Figure 19.- Variation of pitch attitude angle, flight-path angle, and yaw attitude angle with time illustrating behavior of vehicle attitude before and after booster separation.

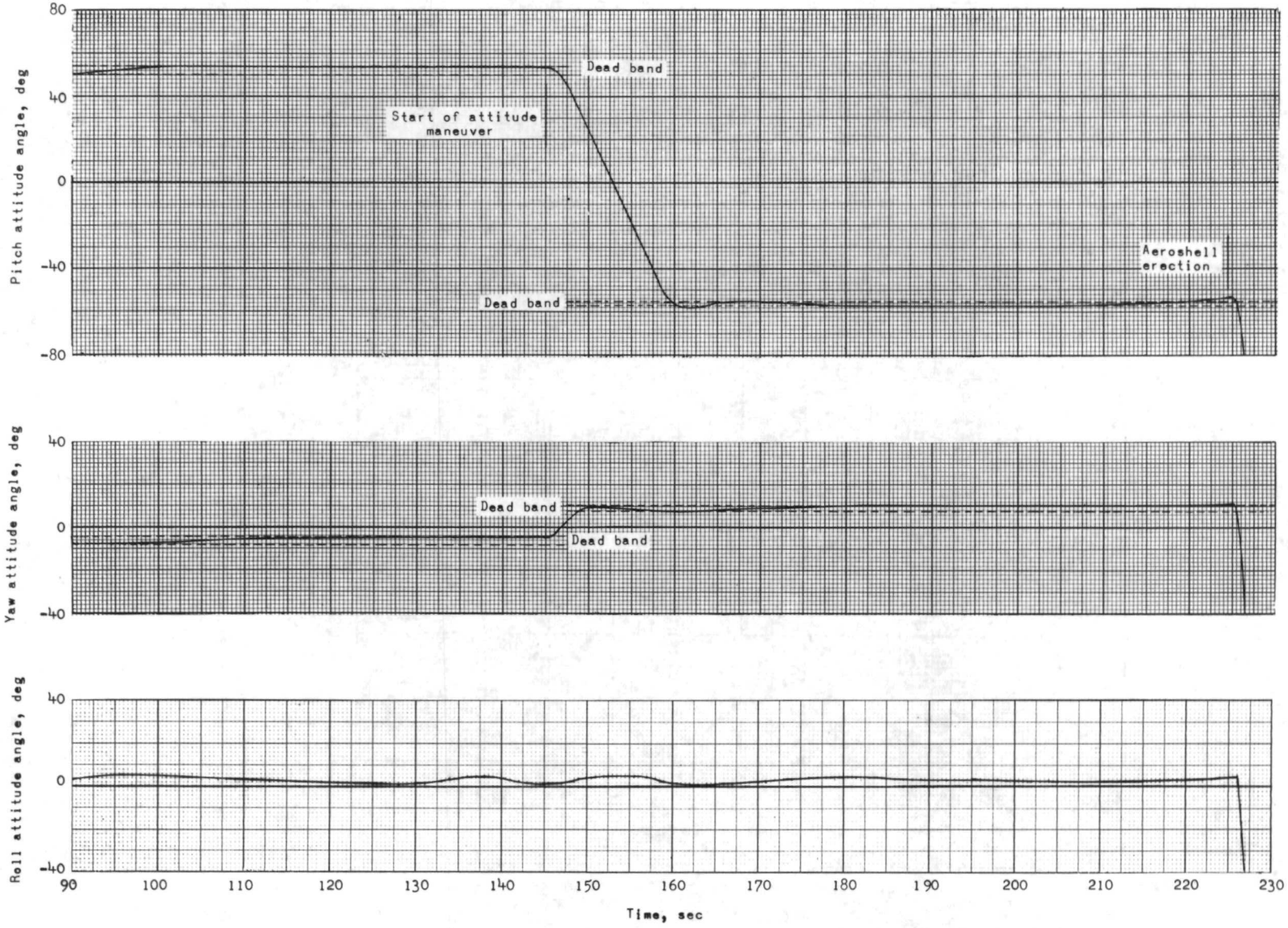

Figure 20.- Variation of pitch, yaw, and roll attitude angles during attitude maneuver.

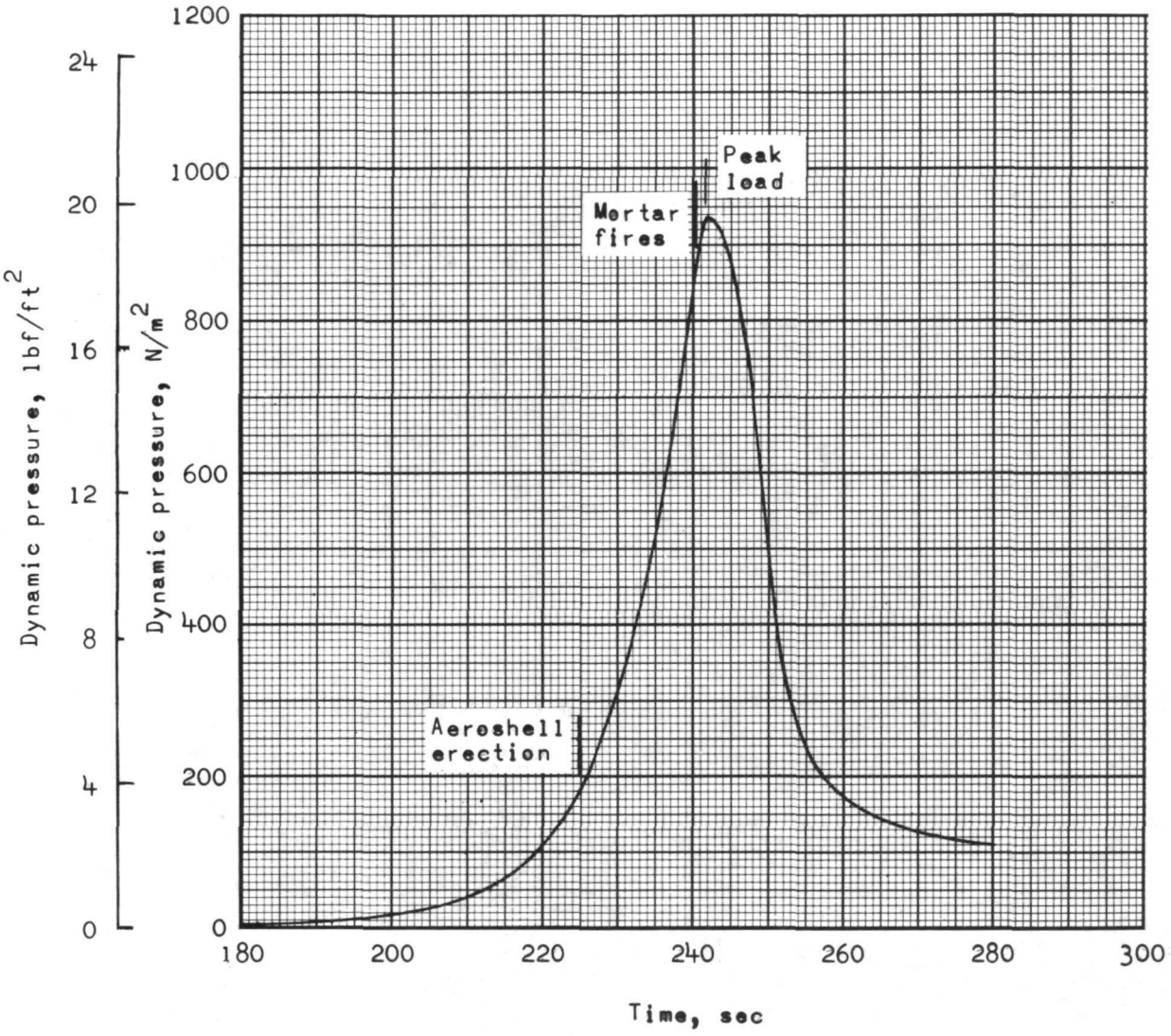

Figure 21.- Variation of dynamic pressure with time during aeroshell erection and parachute test phase.

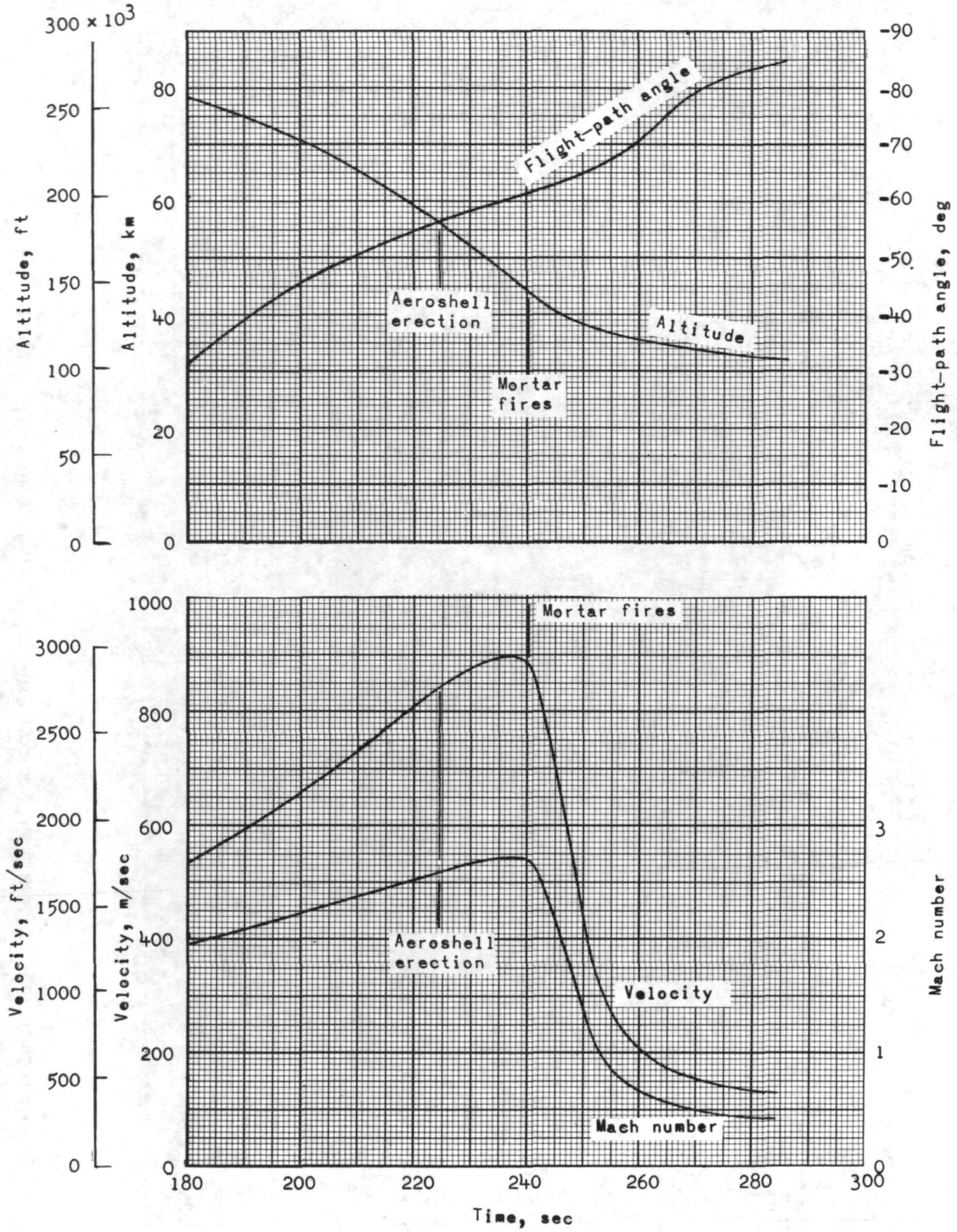

Figure 22.- Variation of flight-path angle, altitude, velocity, and Mach number with time during aeroshell erection and parachute test phase.

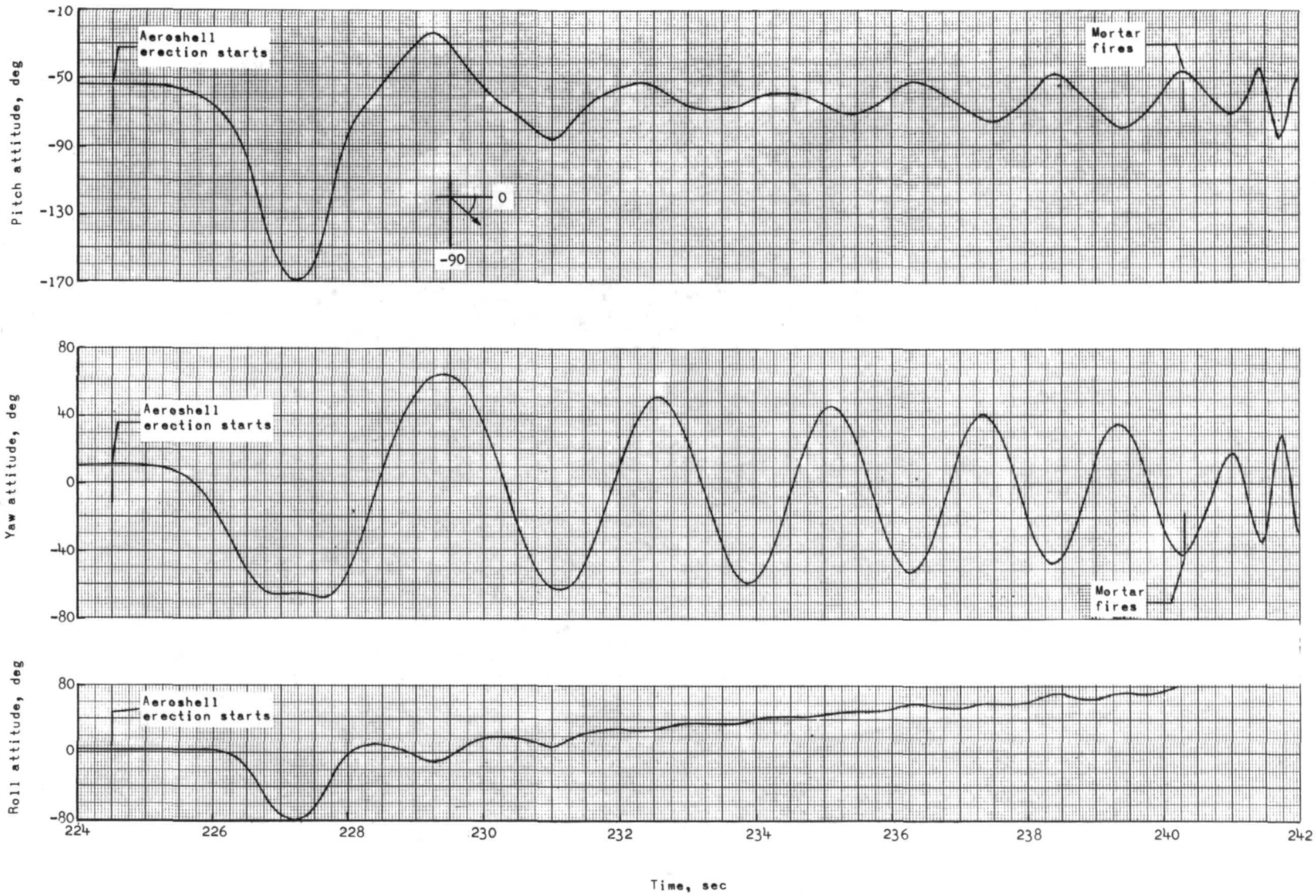

Figure 23.- Variation of attitude in pitch, yaw, and roll with time after aeroshell erection with respect to inertial axis.

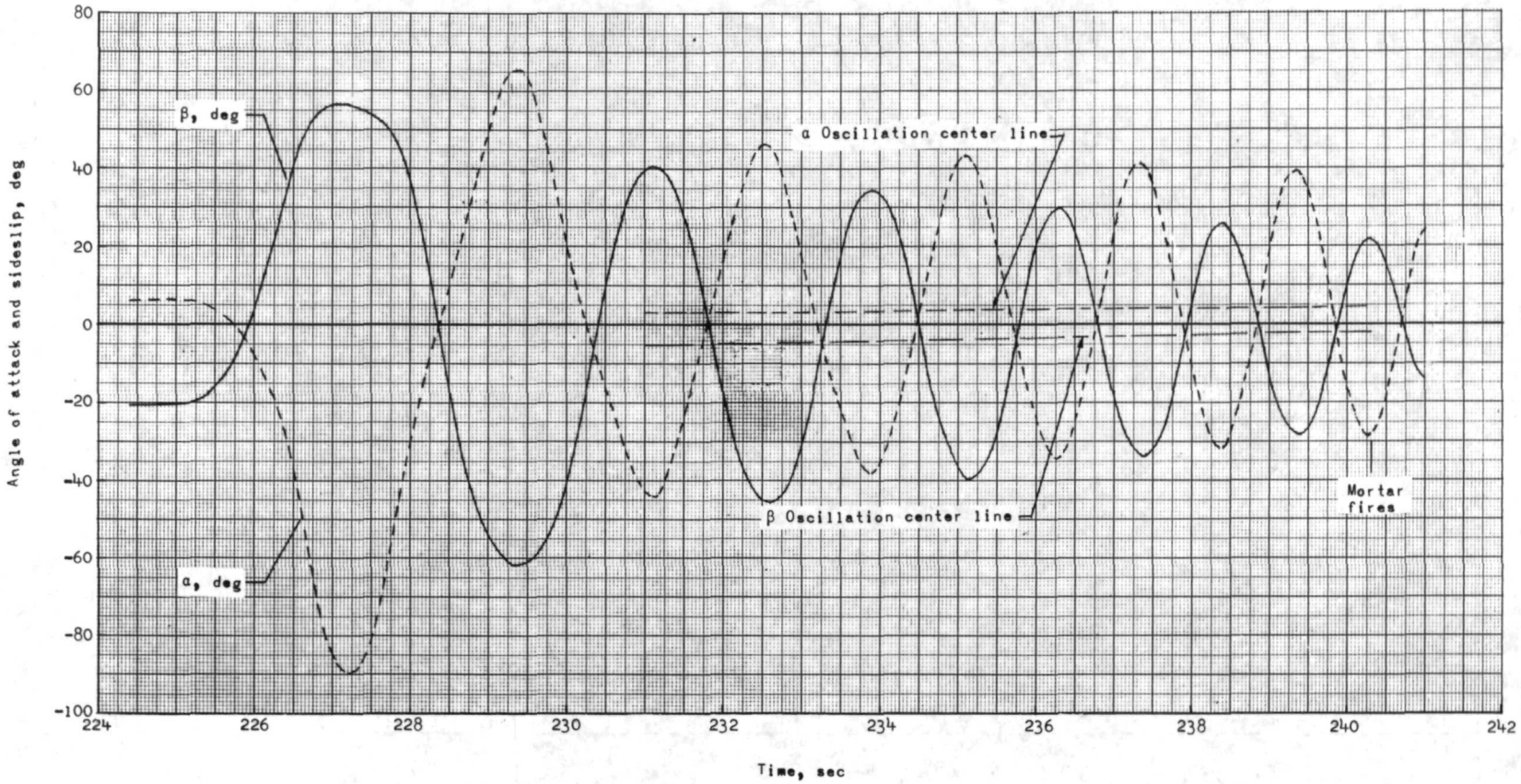

Figure 24.- Variation of angle of attack and sideslip with time as derived from gyro attitude data.

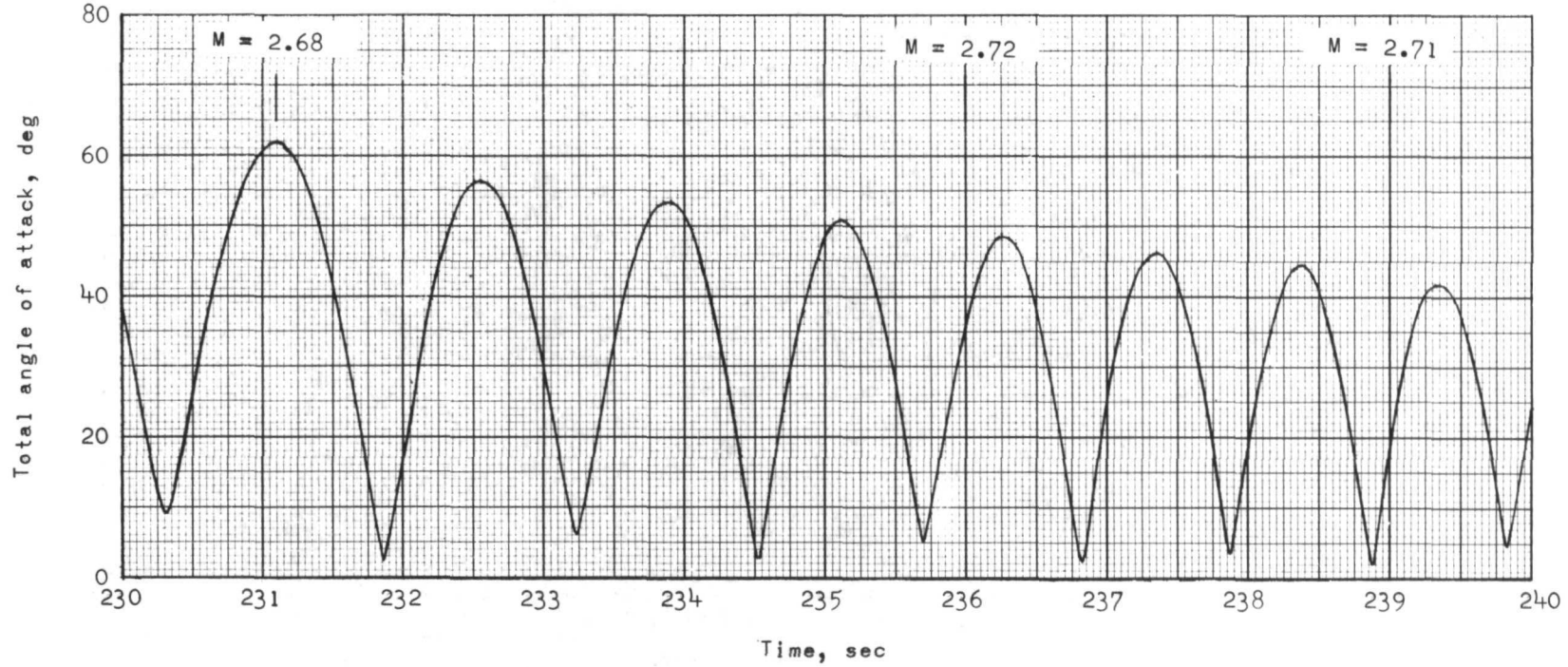

Figure 25.- Variation of total angle of attack with time.

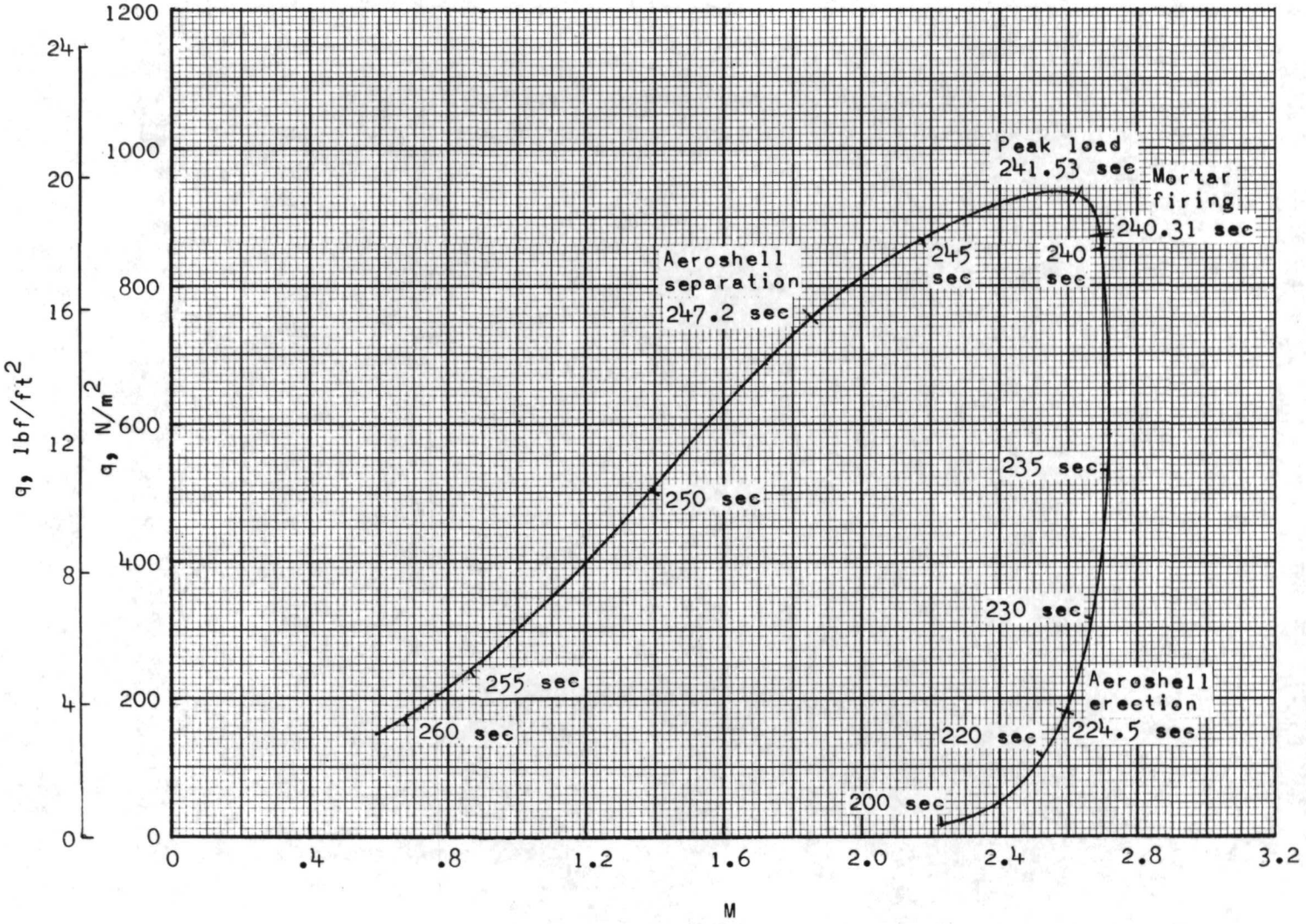

Figure 26.- Variation of dynamic pressure with Mach number from spacecraft entry through parachute test.

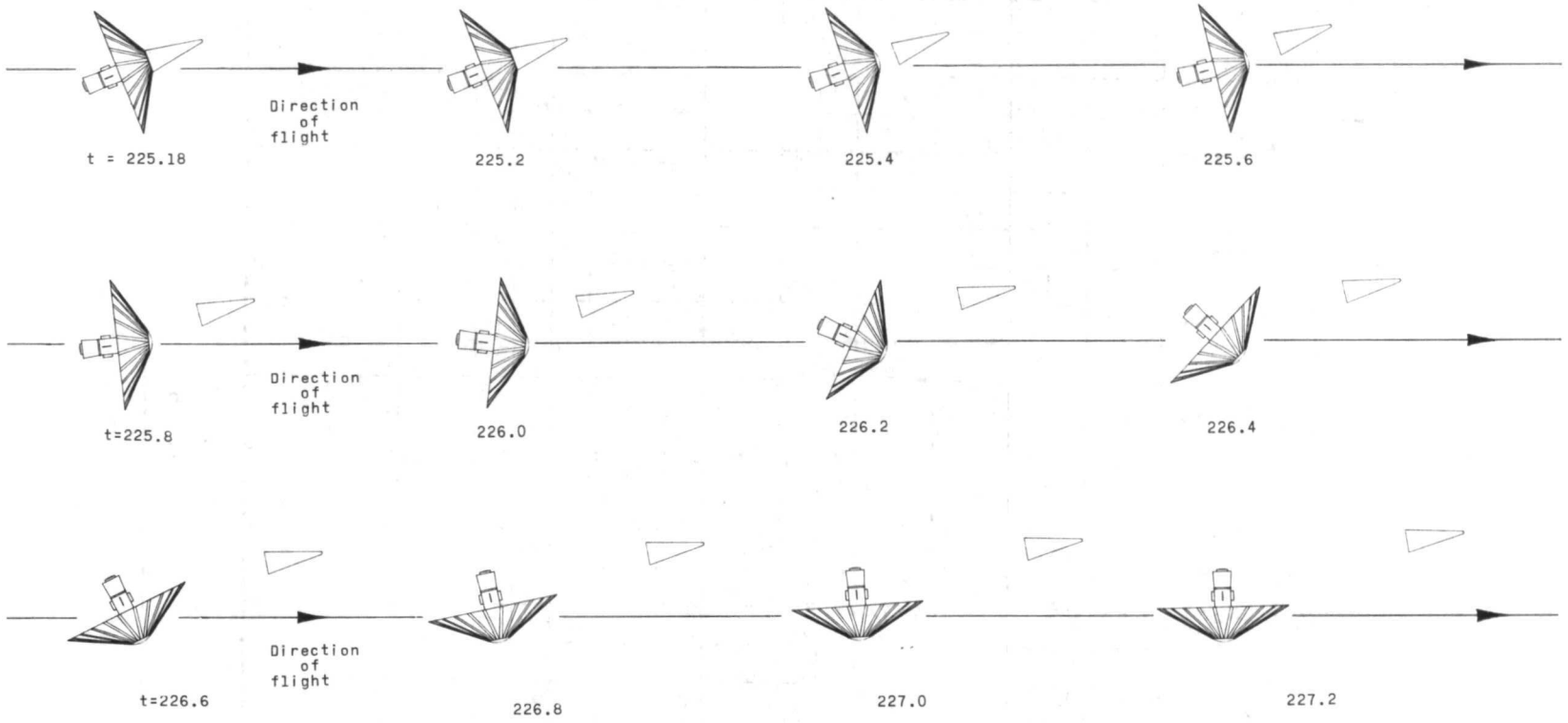

Figure 27.- Time sequence of aeroshell and nose-cone relative position and attitude in oscillation plane after nose-cone separation.

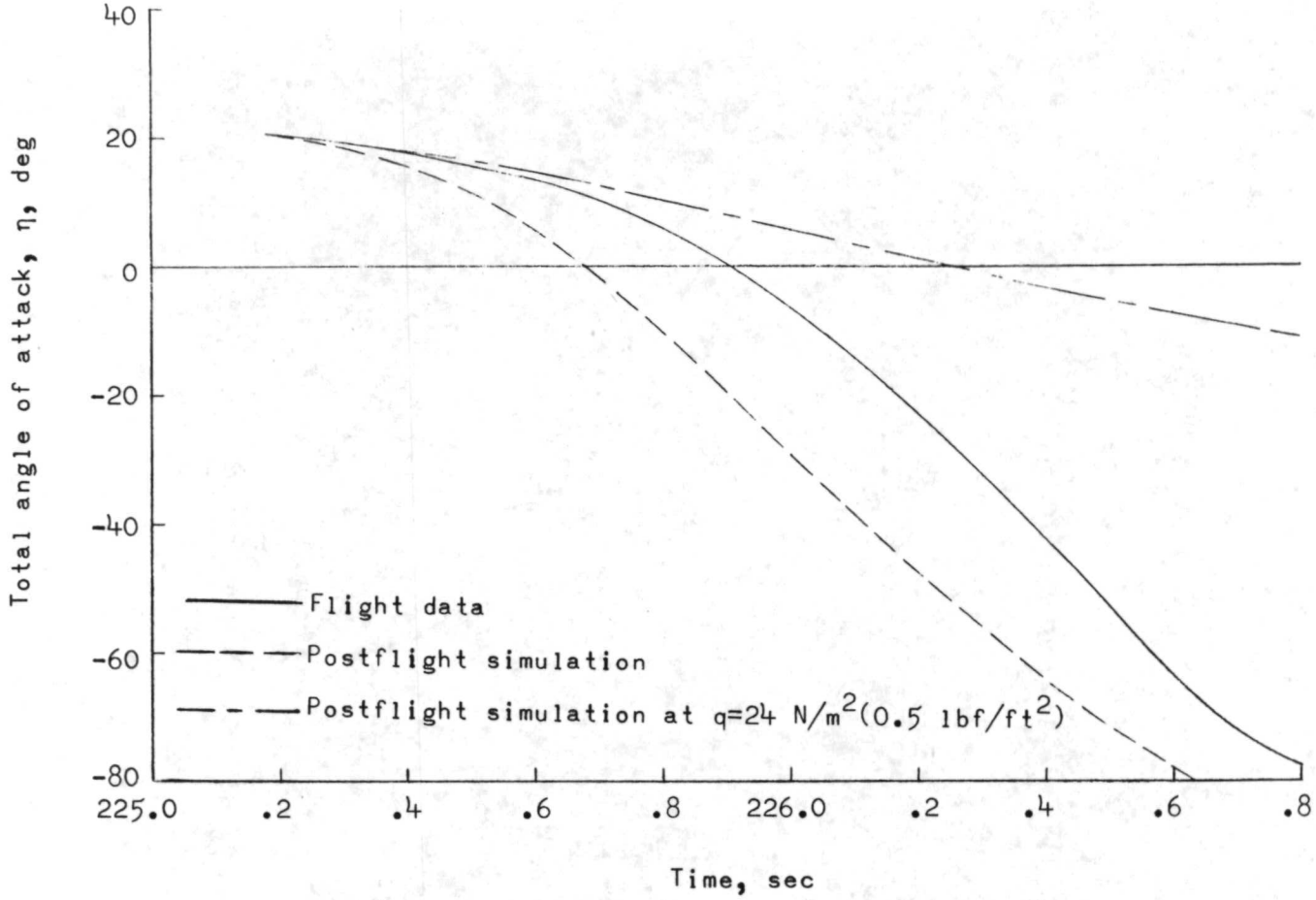

Figure 28.- History of aeroshell total angle of attack η in oscillation plane.

NATIONAL AERONAUTICS AND SPACE ADMINISTRATION
WASHINGTON, D.C. 20546

OFFICIAL BUSINESS
PENALTY FOR PRIVATE USE $300

SPECIAL FOURTH-CLASS RATE BOOK

POSTAGE AND FEES PAID
NATIONAL AERONAUTICS AND SPACE ADMINISTRATION
451

U.S.MAIL

POSTMASTER: If Undeliverable (Section 158 Postal Manual) Do Not Return

"The aeronautical and space activities of the United States shall be conducted so as to contribute . . . to the expansion of human knowledge of phenomena in the atmosphere and space. The Administration shall provide for the widest practicable and appropriate dissemination of information concerning its activities and the results thereof."

—NATIONAL AERONAUTICS AND SPACE ACT OF 1958

NASA SCIENTIFIC AND TECHNICAL PUBLICATIONS

TECHNICAL REPORTS: Scientific and technical information considered important, complete, and a lasting contribution to existing knowledge.

TECHNICAL NOTES: Information less broad in scope but nevertheless of importance as a contribution to existing knowledge.

TECHNICAL MEMORANDUMS: Information receiving limited distribution because of preliminary data, security classification, or other reasons. Also includes conference proceedings with either limited or unlimited distribution.

CONTRACTOR REPORTS: Scientific and technical information generated under a NASA contract or grant and considered an important contribution to existing knowledge.

TECHNICAL TRANSLATIONS: Information published in a foreign language considered to merit NASA distribution in English.

SPECIAL PUBLICATIONS: Information derived from or of value to NASA activities. Publications include final reports of major projects, monographs, data compilations, handbooks, sourcebooks, and special bibliographies.

TECHNOLOGY UTILIZATION PUBLICATIONS: Information on technology used by NASA that may be of particular interest in commercial and other non-aerospace applications. Publications include Tech Briefs, Technology Utilization Reports and Technology Surveys.

Details on the availability of these publications may be obtained from:

SCIENTIFIC AND TECHNICAL INFORMATION OFFICE

NATIONAL AERONAUTICS AND SPACE ADMINISTRATION

Washington, D.C. 20546